GROUNDWATER FLOW IN A VERTICAL PLANE AT THE INTERFACE OF PERMAFROST

By

Sairavichand Paturi, B.tech.

A Thesis Submitted in Partial Fulfillment of the Requirements

for the Degree of

Master of Science

in

Environmental Engineering

University of Alaska Fairbanks

August 2017

APPROVED:

Dr. David L Barnes, Committee Chair
Dr. Mary Beth Leigh, Committee Member
Dr. Yuri Shur, Committee Member
Dr. Leroy Hulsey, Chair
Department of Civil and Environmental Engineering
Dr. Doug J. Goering, Dean
College of Engineering and Mines
Dr. Michael Castellini, *Dean of the Graduate School*

Abstract

Groundwater dynamics in discontinuous permafrost aquifers are complex. The topography of permafrost redirects flow in difficult-to-predict directions that can be tens of degrees off from the regional flow direction. Large zones of permafrost vertically separate aquifers into supra and sub-permafrost portions. The flow dynamics in each portion of the aquifer may be dissimilar due to different controlling boundary conditions. In areas of discontinuities in permafrost, known as open taliks, groundwater in the two portions of the aquifer may mix. These areas of mixing are the focus of this study, in particular, the groundwater dynamics in taliks located in the floodplain of lower reaches of rivers. The study hypothesizes that groundwater flow in floodplain taliks of lower reaches of rivers will bifurcate between the supra and sub-permafrost portions of a discontinuous permafrost aquifer. To test this hypothesis gradient, magnitudes and flow directions were determined at several depths ranging from the water table to 150 ft. (45.7 m) below ground surface, using a linear interpolation scheme in various locations in a floodplain talik. Errors in water level measurements due to instrument errors as well as vertically moving wells were propagated into the gradient calculations by Monte Carlo analysis. Results from this research show that a vertical divide in groundwater flow forms a short distance below the top of permafrost. Groundwater flow above the divide routes into the unconfined supra-permafrost portion of the aquifer. Water below the divide flows into the confined portion of the aquifer below permafrost. The position of the vertical groundwater divide may adjust in relation to the water table position. Additionally, a methodology is presented for stochastically propagating measurement errors into gradient analyses by Monte Carlo analysis. Understanding the flow dynamics in discontinuous permafrost aquifers is key to the understanding of contaminant transport, aquifer recharge, and resource development in subarctic environments.

Table of Contents

Page

List of Figures

Page

List of Tables

Page

Acknowledgments

I started my journey from a country far away to pursue my Master's degree; I got more than I asked for— a life changing experience. I would like to thank my advisor, Dr. David L Barnes; the door was always open whenever I ran into trouble or had a question about the research. He always steered me in the right direction whenever I had a doubt.

Coming from a tropical background, I needed proper guidance in permafrost and the leading problems in Alaska. I would like to thank my wonderful committee members, Dr. Mary Beth and Dr. Yuri Shur who guided my research with their expertise in the field.

The advantage of working in a collaboration project is the ability to meet the best of all the companies involved and I am fortunate to receive help in the field from Mr. Andrew Frick, Environmental Scientist, Shannon & Wilson, Inc. Thanks to Fish, James(james.fish@alaska.gov, 1 August 2017) from Department of Environmental Conservation (DEC) and Jane Paris from Environmental Resources Management (ERM), Inc. for sharing data and providing your valuable support.

I also would like to thank Water and Environmental Research Center(WERC) and Institute of Northern Engineering(INE) for giving me a platform to talk about my research and receive feedback. And the Department of Civil and Environmental Engineering(CEE) for funding me during my program.

Finally, I would like to thank my family and friends for their unconditional love.

Chapter 1 Introduction

Permafrost occupies approximately 13 to 18 percent of underlying exposed land area in the Northern Hemisphere alone, without the account for areas beneath ice caps and ice sheets (Heginbottom et al., 2012). In Alaska, 80 to 90 percent of regions are underlain by permafrost (Heginbottom et al., 2012; Jorgenson et al., 2008). One of the major challenges in permafrost regions is the understanding of groundwater flow. Permafrost zones of Alaska are shown in Figure 1.1 (T. Jorgenson et al., 2008), which shows 80 percent of Alaska underlies permafrost, which includes 32 percent of continuous, 31 percent of discontinuous, 8 percent of sporadic and 10 percent of isolated permafrost. The thickness of permafrost varies from several feet to hundreds of feet. Figure 1.2 from (Brown, 1967) shows the general vertical distribution and thickness of permafrost in different zones. Several factors control the degradation and growth of permafrost including heat transfer from flowing groundwater.

Where large zones of permafrost are present, the frozen ground acts as an impermeable barrier preventing the flow of groundwater vertically (Carlson & Barnes, 2011; Williams, 1970). The aquifer is divided into two main regions: a suprapermafrost groundwater region, which is above the permafrost connected to the active layer and a subpermafrost groundwater region, which is below the permafrost. A talik that connects the suprapermafrost and subpermafrost by completely penetrating through the permafrost is known as open talik, which is mostly associated with rivers or lakes (Sloan et al., 1988). These unfrozen pathways allow the interaction between groundwater and surface water (Mckenzie et al., 2013) The groundwater flow in a discontinuous permafrost region is complex and not well-studied (Hinzman et al., 2006).

Suprapermafrost groundwater flow can channelize between areas of shallow ground surface permafrost (Bolton et al., 2000; Carlson & Barnes, 2011). Areas that experience upward

flowing sub permafrost groundwater through open taliks into the supra permafrost portion of the aquifer result in localized areas of suprapermafrost groundwater recharge. Recharging subpermafrost groundwater results in flow redirection and groundwater mixing. Overall, the topography of the top of permafrost alters suprapermafrost groundwater flow directions in unpredictable directions that can be tens of degrees off of the regional flow direction as found in a study conducted by (Carlson & Barnes, 2011).

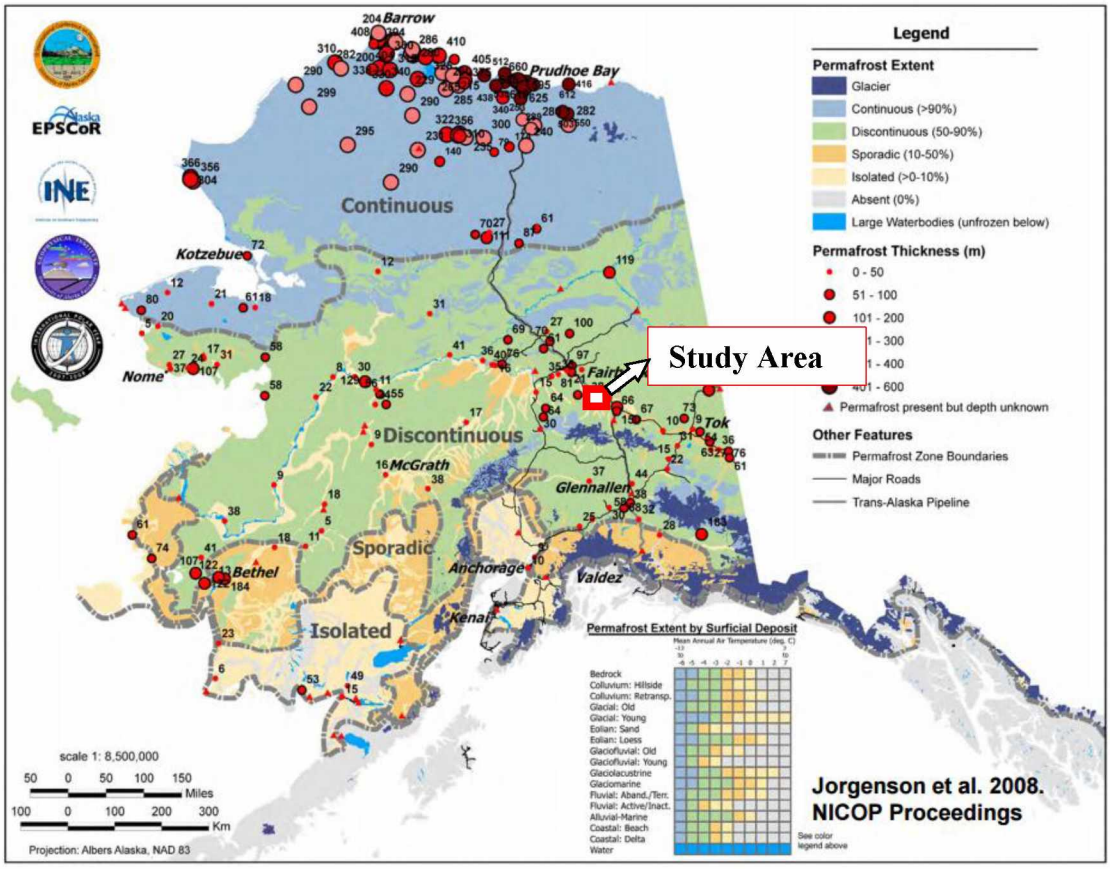

Figure 1.1 Classification of permafrost regions in Alaska with the location of the study site. (T. Jorgenson et al., 2008).

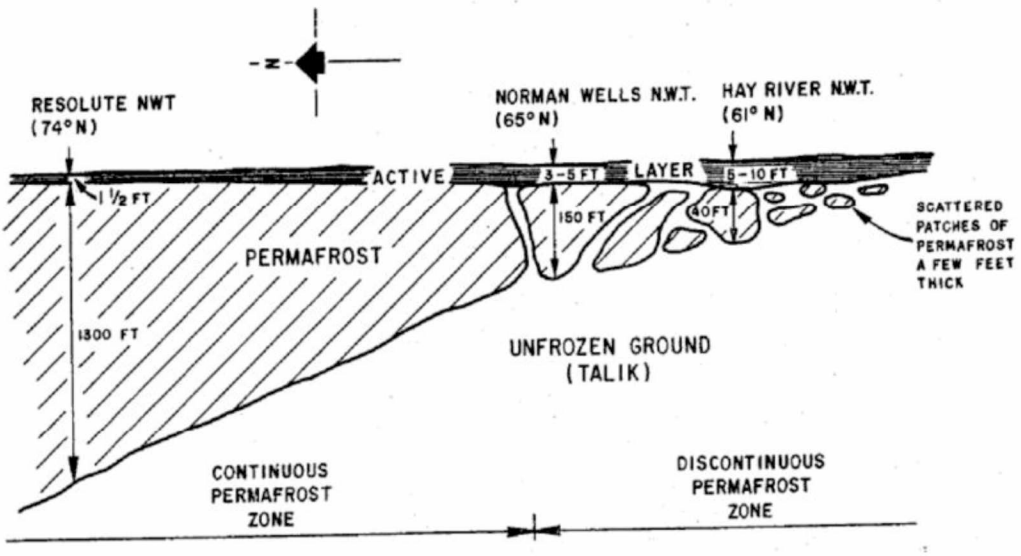

Figure 1.2 Vertical distribution and thickness of permafrost
(Brown, 1967)

Past studies have shown that permafrost is going to impact the flow of groundwater. To date, researchers have only investigated the impact permafrost has on the horizontal flow directions. Very little is understood about the impact permafrost has on the vertical flow of groundwater, particularly in floodplain taliks. Since floodplain taliks are aquifer recharge zones in reaches of losing streams (rivers), an understanding of how permafrost redirects groundwater in these areas is warranted.

1.1 Study Objectives and Hypothesis

This research is focused on understanding the complexity of groundwater flow in discontinuous permafrost, primarily in the vertical direction, as groundwater flows in large open taliks, such as floodplain taliks, interact with permafrost. The study's hypothesis is as follows:

> *As ground water intersects permafrost, the flow will bifurcate into a portion of the water flowing upward into the suprapermafrost portion of the aquifer and the portion being directed downward into the subpermafrost portion of the aquifer.*

Owing to the introduction of possibly large measurement errors due to vertically moving wells caused by freezing and thawing soil, an ancillary objective of this thesis is to define a methodology for propagating water level measurement errors into calculations of the gradient.

1.2 Study Site

The study area is in North Pole, Alaska, which is located in a discontinuous permafrost zone, is shown in Figure 1.1. The site geology under Tanana river, which is recharged with well-stratified silt, sand, and gravel, is classified as a flood-plain talik (Anderson, 1970; Reger et al., 1976). The study site includes a groundwater monitoring well system associated with a contaminant release that occurred at a petroleum refinery located in North Pole, Alaska. The underlying motive of this research is to provide necessary understanding of the transport of contaminated groundwater in discontinuous permafrost aquifers. Portions of this monitoring well system are used to obtain the water level and potentiometric surface measurements necessary to calculate groundwater gradient in three dimensions.

1.3 Conceptual Model for Groundwater Flow at the Interface with Permafrost

Without physical evidence of a possible groundwater flow pattern at the interface with permafrost, the fundamental knowledge of how groundwater flows around low-permeability soils can help to hypothesize a likely flow pattern. Freeze and Witherspoon (1967) used simple two-dimensional numerical groundwater flow simulations to show how heterogeneities influence groundwater flow paths. Following the methodology of these researchers, a simple three-dimensional numerical model bounded by constant head boundaries and lateral no flow boundaries with permafrost represented as a region with very low hydraulic conductivity is created. Results

from this simple model, shown in Figure 1.2, illustrates that the presence of permafrost causes a portion of the flow to separate and flow beneath the permafrost. The horizontal plane that separates the flow of groundwater into the suprapermafrost portion of the aquifer from the subpermafrost portion is known as the vertical groundwater divide. A similar flow pattern is likely in the floodplain talik underneath the North Pole Refinery.

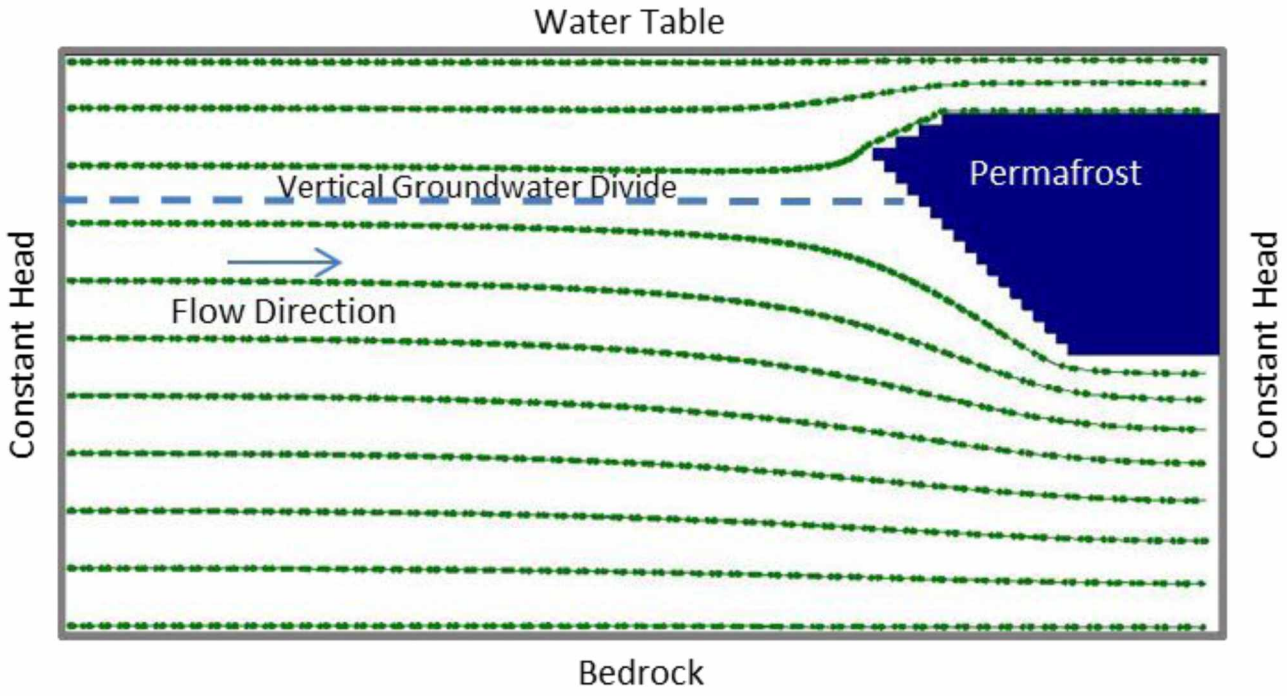

Figure 1.3 Simple numerical model showing groundwater flow around permafrost.
(Green lines are particle pathlines)

Chapter 2 Background

This study is associated with a site characterization of a contaminated aquifer in North Pole, Alaska. Over several decades, a contaminant, 2,3,4,5-tetrahydrothiophene-1,1-dioxide, commonly known as sulfolane, was accidentally released into groundwater from a petroleum refinery located on the floodplain of the Tanana River. Over time the contaminant migrated approximately 3.5 miles downgradient from the source in the suprapermafrost portion of the aquifer. Sulfolane has also migrated into the subpermafrost portion of the aquifer. The objective of this thesis is not necessary to quantify the transport of sulfolane into the subpermafrost aquifer but to quantify the unique groundwater flow dynamics in a floodplain talik— a topic that has not yet been studied. To meet this objective, an understanding of the site and an overall understanding of groundwater flow in permafrost aquifers are needed. Both topics will be presented in this chapter.

2.1 Site Description and its Permafrost Characteristics

The study site is located in a Tanna River flood-plain with an approximate elevation of 146.3 m (480 feet) above mean sea level (AMSL). The area is a discontinuous permafrost zone, which is shown in Figure 1.1. The geological classification is flood-plain alluvium with low ice content and well-stratified silt, sand, and gravel (Anderson, 1970). The configuration of the permafrost in the study site area is complicated; CGG (2013) performed an electromagnetic airborne survey of the area shown in Figure 2.2 and Figure 2.3. Arcadis (2013b) investigated the presence of permafrost using electrical resistivity imaging and frequency domain electromagnetic induction. The undulations in the permafrost topography and presence of open taliks contribute to the complexity in the flow of groundwater both in supra and sub permafrost regions. Both studies show complex configurations of permafrost at the edge of the floodplain talik. Moreover, the study by Arcadis

(2013b) shows smaller bodies of permafrost at sporadic locations in the floodplain talik. The complex pattern of the leading edge of a large zone of permafrost in the floodplain talik and the sporadic presence of small permafrost zones in the floodplain talik will result in complex localized flow patterns, which are much more complex than the simple illustration shown in Figure 1.2. An associated notable result of these surveys is the illustration of the rugged nature of the bottom of permafrost topography. This topography greatly influences the groundwater flow and contaminant transport in the subpermafrost portion of the aquifer as will be discussed in later chapters.

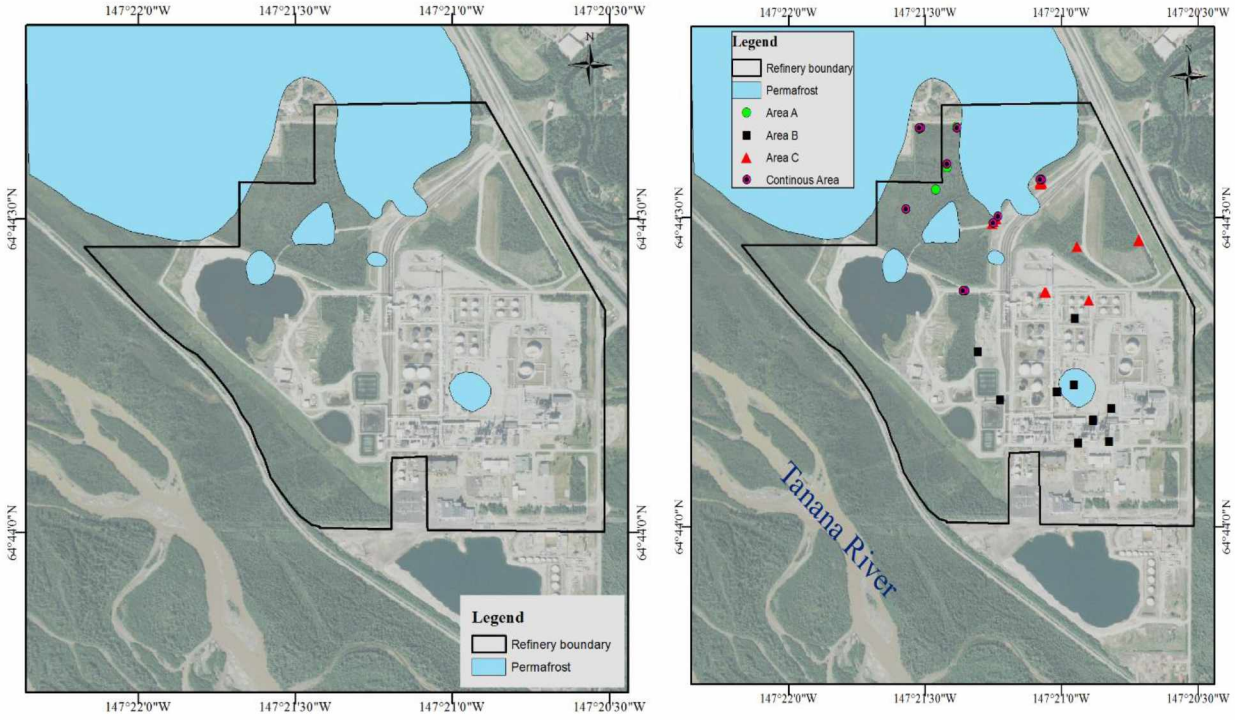

Figure 2.1 Map showing study site
Map on the left shows permafrost and refinery boundary, on the right with monitoring wells in the site

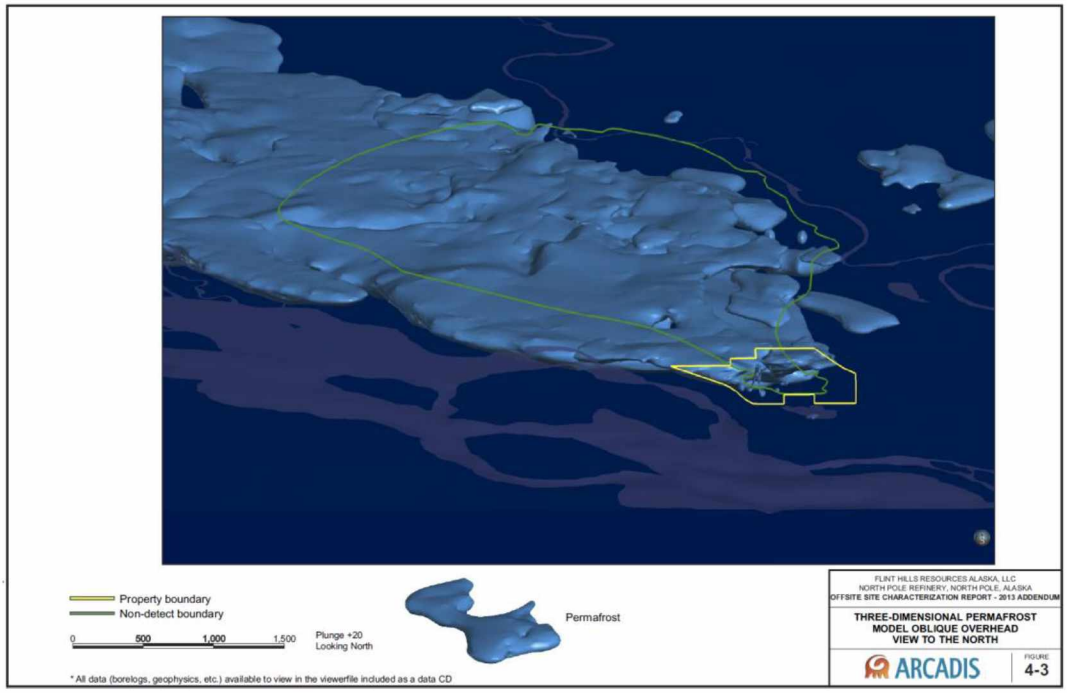

Figure 2.2 Electromagnetic survey results showing the location and topography of top permafrost
(Arcadis 2013b)

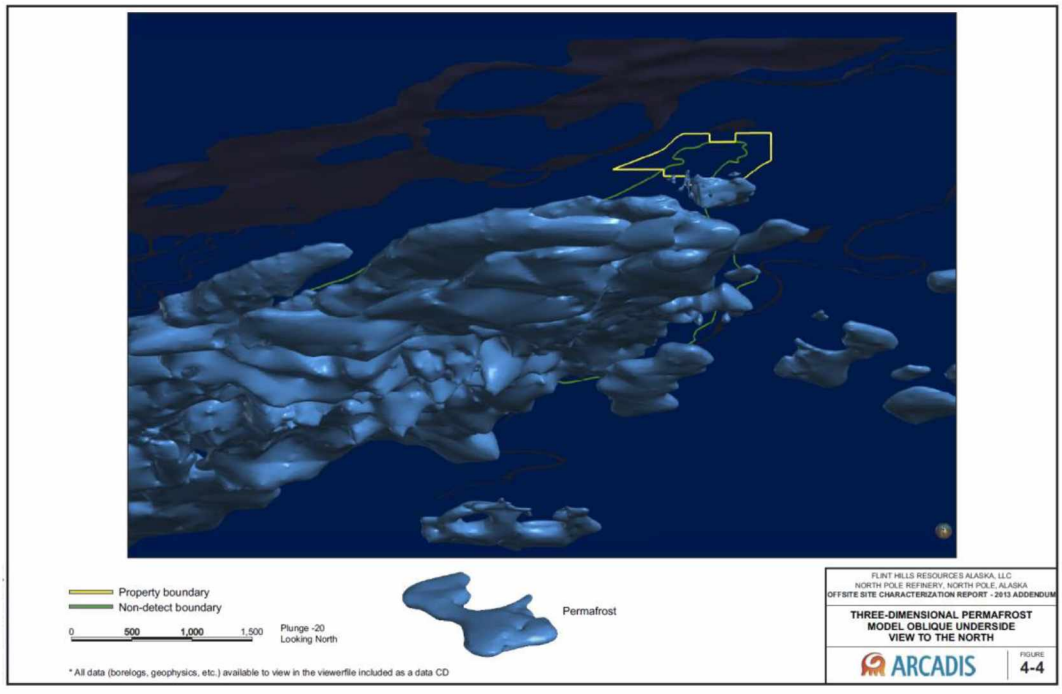

Figure 2.3 Electromagnetic survey results showing topography of bottom permafrost
(Arcadis 2013b)

2.2 Aquifer Characteristic

The predominant recharge of the aquifer comes from Tanana river and small portions of Chena river (Bolton et al., 2000). The majority of the recharge to the suprapermafrost aquifer and upper portion of subpermafrost aquifer is from Tanana River (Barnes, 2014). The Tanana River is the second largest tributary of the Yukon River by area and the basin is bounded on the south by the Alaska Range. Tanana River has an annual discharge of approximately 1172 m^3/s, which is almost 18% of Yukon River annual discharge. (Kraemer et al., 2012). The authors carried out extensive studies using UAR (uranium activity ratio) for the Tanana River and found that the Tanana River water is a mixture of meltwater and two major sources of water with UAR values of 1.10 and 1.43. Based on the results obtained the authors, one could conclude that the Tanana River is fed by two melt water events each year—one early in summer due to snowpack and ice melts and a second influx later in the summer due to glacier melts. The recharge of the deeper layers of sub permafrost region might originate from the Alaska range due to the suprapermafrost groundwater recharge yielding about 1000 to 3000 gallons per minute (Anderson, 1970), which causes the aquifer to develop large groundwater supplies.

2.3 Groundwater in Permafrost Regions

From the research findings of Cederstrom (et al 1963), the upper ground surface in permafrost zones is thawed deep enough to a certain extent during the summer months to create a reservoir of groundwater known as suprapermafrost groundwater. These portions of the aquifer are recharged from snow melt and precipitation events as well as from streams and rivers. In winter, suprapermafrost groundwater may freeze entirely to the top of permafrost. However, in areas of where the top of permafrost is deep from the ground surface, suprapermafrost groundwater may remain unfrozen year round.

The subpermafrost groundwater beneath the permafrost is typically characterized as having long residence times. Recharge for these portions of the aquifer is typically from snow melt and precipitation events at higher elevations, particularly on south facing slopes that are mostly free of permafrost. As this recharge water flows downslope encountering permafrost, a fraction of the water flows underneath permafrost recharging the subpermafrost aquifer. Since open taliks are areas of connection between supra and subpermafrost groundwater, open taliks are also a potential source of subpermafrost recharge. The groundwater that occurs within the thawed zones of permafrost is known as intrapermafrost groundwater, which generally occurs in alluvium or abandoned river channels shown in Figure 2.4. This groundwater is characterized as relatively high salinity, which depresses the freezing point.

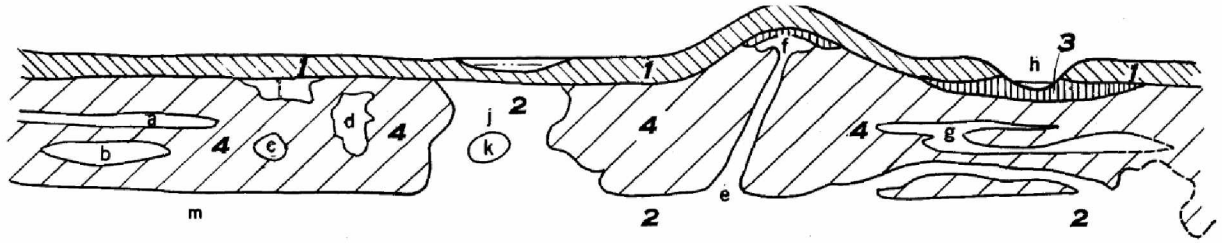

a - Layer type.
b - Lenses, ribbons.
c - Veins, pipes.
d - Block.
e - Crevice-vein type.
f - Hydrolaccolith.
g - Multilayer type.
h - Lake produced by thawing.
i - "Window" of the suprapermafrost thawed layer.
j - "Window" of the completely thawed layer.
k - Island of permafrost.
m - Subpermafrost thawed layer.
1 - Active layer.
2 - "Talik" (thawed) layer.
3 - Ice.
4 - Permafrost.

Figure 2.4 Intrapermafrost water
(Cederstrom et al, 1963)

2.3.1 Groundwater Flow in Flood-plain Talik

According to (Mikhailov, 2008), floodplain taliks are created during convective heat exchange between rivers and floodplains are developed due to the flow of groundwater along a valley slope (Walvoord et al., 2012). Development of taliks has multiple contributing factors such

as the presence of surface water and groundwater discharge. According to the results obtained by Walvoord et al., (2012), taliks play an important role in the circulation of groundwater. For their base case, 76% of total recharge through the ground surface occurs above open taliks while the remaining 24% of recharge enters through the ground surface.

2.3.2 Permafrost Degradation due to Groundwater

According to (Jorgenson et al., 2005), groundwater underlain permafrost areas can cause multiple modes of permafrost degradation. The authors state that groundwater affects permafrost by contributing to heat flow conditions at the subsurface. Furthermore, groundwater is a large factor for permafrost degradation in discontinuous permafrost zones. In colluvial deposits, groundwater flow causes pipes (tunnels) and sinkholes; while in floodplains, the degradation is affected by the subsurface channel gravel (Lawson et al., 1996).

Chapter 3 Methods

To quantify the groundwater dynamics at the interface with permafrost in the floodplain talik of the Tanana River, several monitoring wells from the existing groundwater monitoring system installed by others to characterize and monitor the fate and transport of sulfolane were used to monitor water levels. Groundwater gradients in three dimensions were then calculated using a linear interpolation scheme derived by Abriola et al., (1982). Owing to the vertical movement of monitoring wells due to the freezing and thawing in the active layer, a means of accounting for the error due to the uncertainty in the well elevations (and other marginal errors) was required. The development of this methodology is presented here.

Based on the approximate location of permafrost, the monitoring wells in the study area are grouped into four different localized regions. Three of the four categories were named alphabetically for the convenience of the study: Area A, Area B, Area C is shown in Figure 3.1, and the fourth category is called 'Continuous area' shown in Figure 3.2. To the north edge of the refinery boundary, a major portion of permafrost zone begins after a considerable amount of discontinuity within the refinery. Two areas were selected to delineate the gradient magnitude and flow direction at the edge of the main permafrost zone. These areas are designated Area A and C. The purpose of Area B is to compare the flow pattern upgradient of the permafrost body to the flow at the edge of permafrost. Gradient magnitudes and flow directions were calculated in areas A, B, and C for six different dates spanning from 1Q14, which is the first Quarter of the year 2014. Date of measurement in these quarters are 1Q14 - 03/18/2014 (mm/dd/yy), 2Q14 - 6/11/2014, 3Q14 - 9/09/2014, 4Q14 - 11/20/2014, 1Q15 - 03/18/2015 until 2Q15 - 06/11/2015. Given the propensity for monitoring wells to freeze while closed in this subarctic environment, the 'Continuous area' well location are grouped based on the availability of continuous groundwater

levels for the period of October 2014 to December 2015 while the wells aren't frozen underground. Figure 3.1 and Figure 3.2 show the locations of each well grouping in relation to the North Pole Refinery property boundary, known as permafrost zones and surface water bodies.

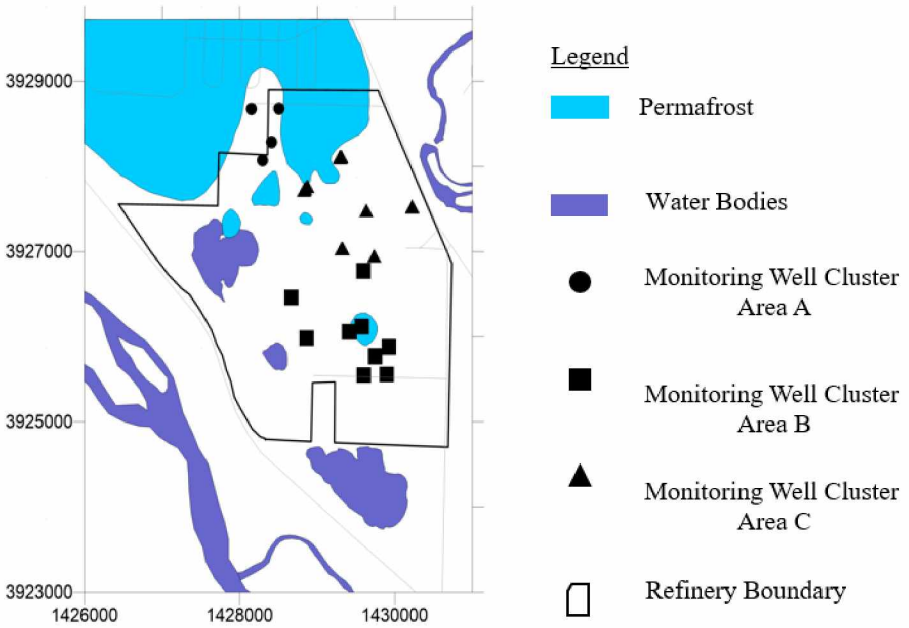

Figure 3.1 Location of Area A, B, and C

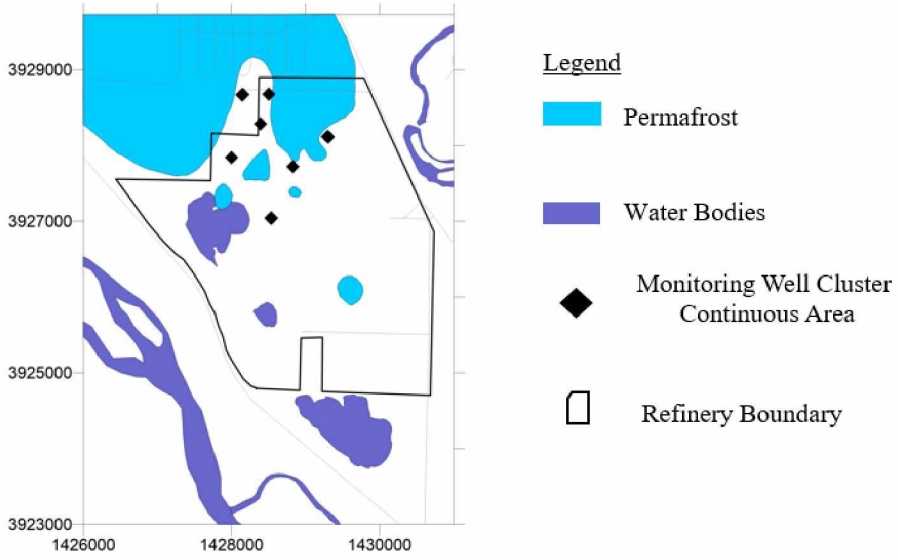

Figure 3.2 Location of Continuous Area

For each area investigated, the gradient magnitude and flow direction at different depths range at the water table as follows: approximately 15 to 20 ft. below ground surface (shallow), approximately 40 to 70 ft. below ground surface (mid shallow), 80 to 90 ft. below ground surface (mid deep) and 150 ft. below ground surface (deep).

3.1 Three-dimensional Vector Analysis

Groundwater flow direction and gradient magnitudes are calculated using vector analysis or linear interpolation for two or three-dimensions (Abriola et al., 1982; Fienen, 2005; Hehlen et al., 2000; Pinder et al., 1981; Silliman et al., 1998; Vacher, 1989). For this study, a linear interpolation method presented by Abriola et al., (1982) was chosen. In this method, water level measurements, or total heads, are obtained from four wells that are positioned in relation to each other such that they form a tetrahedron. Determination of flow gradient in three dimensions is estimated by interpolation using a matrix solution by (Abriola et al., 1982) based on groundwater elevations or hydraulic head values for the four wells which can form a tetrahedron. It is given by,

$$h \cong \hat{h} = \sum_{j=1}^{4} H_j \ \emptyset_j \qquad (1)$$

where H_j is the known head measured at the monitoring wells and $\emptyset_j$ is corresponding linear interpolation function given by $\emptyset_j = a_j + b_j x + c_j y + d_j z$, where a_j, b_j, c_j, d_j are real constant coefficients to be solved for by matrix methods. Knowing these constants, estimates of the hydraulic gradient along the three principal axes ($\partial h/\partial x$, $\partial h/\partial y$, and $\partial h/\partial z$) are as follows:

$$\frac{\partial h}{\partial x} \cong \frac{\partial \hat{h}}{\partial x} = \sum_{j=1}^{4} H_j \ \emptyset_j = \sum_{j=1}^{4} H_j \frac{\partial \emptyset_j}{\partial x} = \sum_{j=1}^{4} H_j \, b_j \qquad (2)$$

$$\frac{\partial h}{\partial y} \cong \frac{\partial \hat{h}}{\partial y} = \sum_{j=1}^{4} H_j \, c_j \tag{3}$$

$$\frac{\partial h}{\partial z} \cong \frac{\partial \hat{h}}{\partial z} = \sum_{j=1}^{4} H_j \, d_j \tag{4}$$

Flow direction is calculated based on the vector position in the quadrant system (Equations 5 and 6). For this study, the horizontal direction is measured clockwise from North (0^0). Vertical is measured from vertically upwards (0^0) resulting in vertically downwards equaling 180^0.

$$Horizontal\ component\ direction\ (\theta h) = \tan^{-1}\left(\frac{\frac{\partial h}{\partial x}}{\frac{\partial h}{\partial y}}\right), in\ degrees \tag{5}$$

$$Vertical\ component\ direction\ (\theta v) = \tan^{-1}\left(\frac{\sqrt{\frac{\partial h^2}{\partial x} + \frac{\partial h^2}{\partial y}}}{\frac{\partial h}{\partial z}}\right), in\ degrees \tag{6}$$

3.2 Data Collection

Area A, B, C and the Continuous well group are sub-grouped into depth ranges. For the continuous well group, pressure-based water level loggers (Onset HOBO U20), also referred to as pressure transducers were installed at known locations below the water level in existing monitoring wells. Each pressure transducer was programmed for hourly water pressure readings. A pressure transducer suspended above the water table in one of the monitoring wells recorded hourly barometric pressure. With these data and the known elevation above mean sea level for each of the monitoring wells, hourly water levels referenced from mean sea level were determined.

The midpoint of the monitoring well screen elevation is the vertical location in space referenced from mean sea level. As the study area is in sub-arctic climatic conditions, deep freezing and thawing ground can cause monitoring wells to move vertically. As ground freezes and ice lenses form, wells tend to move vertically upwards, or 'frost jack'. Thawing ground may result in wells subsiding back into open bore holes due to loss of an adfreeze bond. These seasonal changes in monitoring well elevation are accounted for by quarterly survey of top of well casing (TOC) from which the midpoint screen elevation changes can be calculated.

The data are separated based on wells grouped under Area A, Area B, Area C and Continuous. The geographic location of the monitoring wells, top of casing and moment in time water levels are shared are recorded in the quarterly reports generated by Arcadis NV (a company working on the study area) for Flint Hills Resources Alaska, LLC and North Pole Refinery, North Pole, Alaska. The monitoring well identification is given based on the total number of wells in the study area and is represented in the order of monitoring well (MW), numerical ID of the well, and approximate bottom depth of the monitoring well in feet.

A total of sixteen monitoring wells are grouped under Area A, with the shallow well depth of 15 feet, mid-shallow well depth ranging 55 to 65 feet, mid deep well ranging 80 to 90 feet and deep wells until 150 feet. These wells are in close proximity to the permafrost zone under the surface below the ground. Table 3.1 gives the geographic location (Easting and Northing) of these wells, which is recorded in US Survey feet. The midpoint of the well screen elevations, which are corrected based on the Top of casing changes measured quarterly, is given in Table3.2. Groundwater levels measured at these moments in time for the respective quarters are given in Table 3.3.

Table 3.1 Location of Area A Monitoring Wells

Well depth range	Well ID	Easting [a]	Northing [a]
Shallow Wells (15 ft. bgs [b])	MW 364-15	1428505	3928680
	MW 148-15	1428153	3928675
	MW 359-15	1428297	3928071
	MW 360-15	1428409	3928286
Mid Shallow Wells (50-65 ft. bgs)	MW 364-65	1428509	3928671
	MW 148-55	1428140	3928671
	MW 359-60	1428304	3928073
	MW 360-50	1428397	3928287
Mid Deep Wells (80-90 ft. bgs)	MW 364-90	1428508	3928675
	MW 148-80	1428142	3928677
	MW 359-80	1428292	3928066
	MW 360-80	1428416	3928287
Deep Wells (150 ft. bgs)	MW 364-150	1428504	3928671
	MW 148-150	1428147	3928673
	MW 359-150	1428310	3928075
	MW 360-150	1428392	3928288

[a] Data obtained from (ARCADIS, 2015a) in US Survey ft., [b] bgs = below ground surface

Table 3.2 Screen Depths of Area A Monitoring Wells for Each Quarter Analyzed

Well depth range	Well ID	Well Screen Midpoint Elevations[a] (ft. amsl [c])					
		1Q14[d]	2Q14	3Q14	4Q15	1Q15	2Q15
Shallow Wells (15 ft. bgs [b])	MW 364-15	481.20	481.63	481.63	481.63	481.63	481.83
	MW 148-15	481.30	481.29	481.97	482.22	482.39	482.41
	MW 359-15	481.87	481.87	481.87	481.87	481.93	481.92
	MW 360-15	481.80	481.80	481.80	481.79	481.90	481.57
Mid Shallow Wells (50-65 ft. bgs)	MW 364-65	428.65	428.56	428.56	428.78	428.78	428.78
	MW 148-55	438.15	438.29	438.31	438.38	438.70	438.39
	MW 359-60	434.24	434.24	434.24	434.27	434.32	434.32
	MW 360-50	444.08	444.08	444.08	444.21	444.32	444.33
Mid Deep Wells (80-90 ft. bgs)	MW 364-90	404.09	404.07	404.07	404.24	404.24	404.24
	MW 148-80	412.72	412.73	412.75	412.76	412.87	412.86
	MW 359-80	414.50	414.50	414.50	414.52	414.58	414.56
	MW 360-80	414.69	414.69	414.69	414.67	414.74	414.71
Deep Wells (150 ft. bgs)	MW 364-150	343.60	343.53	343.53	343.71	343.71	343.71
	MW 148-150	342.22	342.24	342.26	342.25	342.23	342.27
	MW 359-150	344.36	344.36	344.36	344.35	344.41	344.39
	MW 360-150	344.59	344.59	344.59	344.63	344.72	344.66

[a] Calculated based on data obtained from. (ARCADIS, 2014a)(ARCADIS, 2014b)(ARCADIS, 2014c) (ARCADIS, 2014d)(ARCADIS, 2015a), [b] bgs = below ground surface, [c] amsl = above mean sea level, [d] 1Q14 format represents 1=first Q=Quarter 14= year 2014

Table 3.3 Groundwater elevations measured on discrete dates for Area A Monitoring Wells

Well depth range	Well ID	Groundwater Elevation [a] (ft. amsl [c])					
		1Q14 [d]	2Q14	3Q14	4Q14	1Q15	2Q15
Shallow Wells (15 ft. bgs [b])	MW 364-15	482.47	482.89	484.01	483.11	482.56	483.16
	MW 148-15	482.49	482.98	484.18	483.07	482.76	483.15
	MW 359-15	483.06	483.45	484.57	483.85	483.26	483.71
	MW 360-15	482.90	483.29	484.44	483.62	483.13	483.59
Mid Shallow Wells (50-65 ft. bgs)	MW 364-65	482.57	482.93	484.68	483.39	482.91	484.68
	MW 148-55	482.48	483	484.08	483.22	482.79	484.08
	MW 359-60	483.05	483.43	484.56	483.72	483.31	484.56
	MW 360-50	482.78	483.16	484.3	483.39	483.12	484.3
Mid Deep Wells (80-90 ft. bgs)	MW 364-90	482.50	482.92	484.36	483.37	482.84	483.23
	MW 148-80	482.55	482.93	484.8	483.2	482.76	483.12
	MW 359-80	483.00	483.4	484.54	483.69	483.25	483.68
	MW 360-80	482.90	483.31	484.46	483.6	483.14	483.58
Deep Wells (150 ft. bgs)	MW 364-150	482.55	482.9	484.36	483.36	482.93	482.9
	MW 148-150	482.57	482.98	484.1	483.23	482.76	482.98
	MW 359-150	483.01	483.43	484.55	483.75	483.28	483.43
	MW 360-150	482.83	483.28	484.42	483.56	483.17	483.28

[a] Data obtained from. (ARCADIS, 2014a)(ARCADIS, 2014b)(ARCADIS, 2014c)(ARCADIS, 2014d) (ARCADIS, 2015a), [b] bgs = below ground surface, [c] amsl = above mean sea level, [d] 1Q14 format represents 1=first Q=Quarter 14= year 2014

Area B is grouped with twelve monitoring wells where the shallow well depth is 15 to 20 feet, mid-shallow well depth ranging 50 to 65 feet, mid deep wells at 90 feet. The geographic location, which is recorded in US survey feet, are mentioned in Table 3.4. Midpoint screen elevations are shown in Table 3.5. Groundwater levels measured at these moments in time for the respective quarters are given in Table 3.6 where some of the wells that are frozen due to the sub-arctic conditions are also mentioned.

Table 3.4 Location of Area B Monitoring Wells

Well depth range	Well ID	Easting [a]	Northing [a]
Shallow Wells (15-20 ft. bgs [b])	MW-367-15	1429601	3925546
	MW-176-15	1429416	3926056
	MW-336-20	1429746	3925764
	MW-361-15	1429896	3925554
Mid Shallow Wells (50-65 ft. bgs)	MW-180-50	1429923	3925880
	MW-176-50	1429412	3926056
	MW-110-65	1428865	3925984
	MW-336-55	1429749	3925773
Mid Deep Wells (90 ft. bgs)	MW-178-90	1429574	3926117
	MW-175-90	1429593	3926774
	MW-174-90	1428664	3926461
	MW-176-90	1429408	3926057

[a] Data obtained from (ARCADIS, 2015a) in US Survey ft., [b] bgs = below ground surface

Table 3.5 Screen Depths of Area B Monitoring Wells for Each Quarter Analyzed

Well depth range	Well ID	Well Screen Midpoint Elevations[a] (ft. amsl [c])					
		1Q14 [d]	2Q14	3Q14	4Q15	1Q15	2Q15
Shallow Wells (15-20 ft. bgs [b])	MW 367-15	483.75	483.75	483.75	483.75	483.75	483.75
	MW 176-15	484.33	484.38	484.38	484.38	484.38	484.38
	MW 336-20	475.74	475.74	475.74	475.74	475.74	475.74
	MW 361-15	483.97	483.97	483.97	483.97	483.97	483.97
Mid Shallow Wells (50-65 ft. bgs)	MW 180-50	446.26	446.30	446.30	446.30	446.30	446.30
	MW 176-50	446.06	446.09	446.09	446.09	446.09	446.09
	MW 110-65	430.86	430.82	430.82	430.82	430.82	430.82
	MW 336-55	440.64	440.64	440.64	440.64	440.64	440.64
Mid Deep Wells (90 ft. bgs)	MW 178-90	404.09	404.07	404.07	404.24	404.24	404.24
	MW 175-90	412.72	412.73	412.75	412.76	412.87	412.86
	MW 174-90	414.50	414.50	414.50	414.52	414.58	414.56
	MW 176-90	414.69	414.69	414.69	414.67	414.74	414.71

[a] Calculated based on data obtained from. (ARCADIS, 2014a)(ARCADIS, 2014b)(ARCADIS, 2014c)(ARCADIS, 2014d)(ARCADIS, 2015a), [b] bgs = below ground surface, [c] amsl = above mean sea level, [d] 1Q14 format represents 1=first Q=Quarter 14= year 2014

Table 3.6 Groundwater elevations measured on discrete dates for Well Area B

Well depth range	Well ID	Groundwater Elevation [a] (ft. amsl [c])					
		1Q14 [d]	2Q14	3Q14	4Q14	1Q15	2Q15
Shallow Wells (15-20 ft. bgs [b])	MW-367-15	Frozen (MW 336-20)	485.76	487.04	486.27	Frozen (MW 336-20)	486.12
	MW-176-15		485.26	486.52	485.74		485.65
	MW-336-20		485.48	487.01	486.21		485.9
	MW-361-15		486.02	487.34	486.55		486.53
Mid Shallow Wells (50-65 ft.. bgs)	MW-180-50	Frozen (MW 336-55)	Frozen (MW 336-55)	487.00	486.19	Frozen (MW 176-50 MW 336-55)	486.16
	MW-176-50			486.61	485.82		485.73
	MW-110-65			486.29	485.53		485.38
	MW-336-55			487.03	486.24		485.86
Mid Deep Wells (80-90 ft. bgs)	MW-178-90	484.93	484.38	486.64	485.89	Frozen (MW 176-90 MW 178-90)	485.66
	MW-175-90	484.15	484.66	485.92	485.01		484.97
	MW-174-90	484.23	484.64	485.81	485.03		484.98
	MW-176-90	484.93	484.66	486.62	485.86		485.76

[a] Data obtained from. (ARCADIS, 2014a)(ARCADIS, 2014b)(ARCADIS, 2014c)(ARCADIS, 2014d) (ARCADIS, 2015a), [b] bgs = below ground surface, [c] amsl = above mean sea level, [d] 1Q14 format represents 1=first Q=Quarter 14= year 2014

Twelve monitoring wells are grouped in Area C, with the shallow well depth of 15 feet, mid deep wells at 70 to 90 feet and deep wells at 150 feet. The locations, recorded in US survey feet, are mentioned in Table 3.7 and midpoint screen elevations are shown in Table 3.8. Groundwater levels

measured at these moments in time for the respective quarters are given in Table 3.9 where some of the wells that are frozen due to the sub-arctic conditions are also mentioned.

Table 3.7 Location of Area C Monitoring Wells

Well depth range	Well ID	Easting [a]	Northing [a]
Shallow Wells (15 ft. bgs [b])	MW-306-15	1429601	3925546
	MW-173-15	1429416	3926056
	MW-334-15	1429746	3925764
	MW-304-15	1429896	3925554
Mid Deep Wells (70-90 ft. bgs)	MW-306-70	1429309	3928116
	MW-144-90	1429632	3927483
	MW-334-85	1429315	3927037
	MW-304-80	1428844	3927741
Deep Wells (150 ft. bgs)	MW-306-150	1429294	3928118
	MW-173-150	1430222	3927527
	MW-307-150	1429735	3926952
	MW-304-150	1428871	3927769

[a] Data obtained from (ARCADIS, 2015a) in US Survey ft., [b] bgs = below ground surface

Table 3.8 Screen Depths of Area C Monitoring Wells for Each Quarter Analyzed

Well depth range	Well ID	Well Screen Midpoint Elevations[a] (ft. amsl [c])					
		1Q14[d]	2Q14	3Q14	4Q15	1Q15	2Q15
Shallow Wells (15 ft. bgs[b])	MW 306-15	483.44	483.43	483.43	483.43	483.43	483.60
	MW 173-15	483.59	483.67	483.67	483.67	483.67	483.67
	MW 334-15	483.29	483.26	483.27	483.29	483.31	483.34
	MW 304-15	480.69	480.69	480.69	480.72	480.73	480.73
Mid Deep Wells (70-90 ft. bgs)	MW 306-70	425.40	425.40	425.40	425.39	425.39	425.39
	MW 144-90	404.43	404.45	404.45	404.45	404.45	404.45
	MW 334-85	410.29	410.30	410.30	410.29	410.28	410.32
	MW 304-80	415.69	415.71	415.72	415.72	415.73	415.72
Deep Wells (150 ft. bgs)	MW 306-150	345.87	345.87	345.87	345.88	345.88	345.87
	MW 173-150	345.07	345.13	345.13	345.13	345.13	345.13
	MW 307-150	345.65	345.65	345.65	345.64	345.64	345.66
	MW 304-150	346.24	346.25	346.24	346.25	346.27	346.26

[a] Calculated based on data obtained from. (ARCADIS, 2014a)(ARCADIS, 2014b)(ARCADIS, 2014c)(ARCADIS, 2014d)(ARCADIS, 2015a), [b] bgs = below ground surface, [c] amsl = above mean sea level, [d] 1Q14 format represents 1=first Q=Quarter 14= year 2014

Table 3.9 Groundwater elevations measured on discrete dates for Well Area C

Well depth range	Well ID	Groundwater Elevation [a] (ft. amsl [c])					
		1Q14 [d]	2Q14	3Q14	4Q14	1Q15	2Q15
Shallow Wells (15 ft.. bgs [b])	MW-306-15	Frozen (MW 173-15)	483.59	484.89	483.91	483.45	483.87
	MW-173-15		484.15	485.58	484.5	483.88	484.39
	MW-334-15		484.03	485.18	484.39	483.77	484.25
	MW-304-15		483.73	484.94	484.08	483.58	484.03
Mid Deep Wells (70-90 ft. bgs)	MW-306-70	483.15	483.55	484.73	483.86	483.39	483.84
	MW-144-90	483.65	484.11	485.4	484.5	483.97	484.38
	MW-334-85	483.92	484.03	485.58	484.72	484.19	484.66
	MW-304-80	483.35	483.75	484.93	484.12	483.61	484.05
Deep Wells (150 ft. bgs)	MW-306-150	483.08	483.52	484.74	483.85	Frozen (MW 307-150)	483.8
	MW-173-150	483.72	484.3	485.71	484.69		484.58
	MW-307-150	484.16	484.59	485.89	484.97		484.93
	MW-304-150	483.37	483.77	484.98	484.12		484.07

[a] Data obtained from. (ARCADIS, 2014a)(ARCADIS, 2014b)(ARCADIS, 2014c)(ARCADIS, 2014d) (ARCADIS, 2015a), [b] bgs = below ground surface, [c] amsl = above mean sea level, [d] 1Q14 format represents 1=first Q=Quarter 14= year 2014

The location and midpoint elevations of the twelve monitoring wells that are grouped for Continuous are given in Table 3.10 and Table 3.11. For the groundwater levels, the hourly pressure transducer data from October 2014 to December 2015 has been collected for analysis. A detailed explanation of the groundwater level changes with respect to time is discussed in the results section.

Table 3.10 Monitoring Wells used for Continuous Area

Well depth range	Well ID	Easting [a]	Northing [a]
Shallow Wells (15 ft. bgs [b])	MW 148-15	1428153	3928675
	MW 304-15	1428505	3928680
	MW 364-15	1428828	3927724
	MW 309-15	1428539	3927043
Mid Shallow Wells (40-70 ft. bgs)	MW 358-40	1428002	3927842
	MW 309-66	1428532	3927043
	MW 306-70	1429309	3928116
	MW 148-55	1428140	3928671
Deep Wells (150 ft. bgs)	MW 306-150	1429294	3928118
	MW 360-150	1428392	3928288
	MW 358-150	1427992	3927835
	MW 304-150	1428871	3927769

[a] Data obtained from (ARCADIS, 2015a) in US Survey ft., [b] bgs = below ground surface

Table 3.11 Screen Depths of Continuous Area Monitoring Wells for Each Quarter Analyzed

Well depth range	Well ID	Well Screen Midpoint Elevations[a] (ft. amsl [c])				
		4Q14 [d]	1Q15	2Q15	3Q15	4Q15
Shallow Wells (15 ft. bgs [b])	MW 148-15	482.22	482.39	482.41	482.41	482.01
	MW 304-15	480.72	480.73	480.73	480.58	480.59
	MW 364-15	481.63	481.63	481.83	481.55	481.55
	MW 309-15	482.25	482.27	482.25	482.54	482.26
Mid Shallow Wells (40-70 ft. bgs)	MW 358-40	454.87	454.93	454.94	454.91	454.93
	MW 309-66	430.26	430.28	430.27	430.15	430.13
	MW 306-70	425.39	425.39	425.39	425.39	425.40
	MW 148-55	438.38	438.70	438.39	437.95	437.95
Deep Wells (150 ft. bgs)	MW 306-150	345.88	345.88	345.87	345.87	345.88
	MW 360-150	344.63	344.72	344.66	344.66	344.65
	MW 358-150	344.33	344.40	344.33	344.30	344.33
	MW 304-150	346.25	346.27	346.26	346.24	346.26

[a] Calculated based on data obtained from. (ARCADIS, 2014a)(ARCADIS, 2014b)(ARCADIS, 2014c)(ARCADIS, 2014d)(ARCADIS, 2015a), [b] bgs = below ground surface, [c] amsl = above mean sea level, [d] 4Q14 format represents 4=fourth Q=Quarter 14= year 2014

3.3 Errors in Groundwater Level Measurements.

Every groundwater level measurement is associated with certain marginal errors taken with some form of a length or distance measuring device such as a water level meter or a length measurement of a cable used to suspend a pressure transducer in a monitoring well. The magnitude of these errors can range from minimum value to high value due to a combination of the errors introduced by a vertical well. For this study, its is required to determine the resulting marginal error in gradient magnitude and flow direction when the water level measurement errors are asymmetrical, such as in the case when water level measurements are obtained from frost heaving and thaw subsiding monitoring wells. The following information is a discussion of the errors that make up the total error in water level measurements, the resulting marginal error equations when symmetrical water level measurement errors are propagated into the Abriola and Pinder (1982) method for determining gradient (the deterministic approach), a discussion on the Monte Carlo approach to determining the marginal error in gradient when errors in water level measurements

are asymmetrical (stochastic approach), and finally a comparison between the deterministic approach and stochastic approach to determine the appropriate statistics to use for characterization of the best estimate and marginal error in gradient and flow direction. A detailed explanation is discussed in following sections based on (Barnes, 2017) unpublished work.

3.3.1 Pressure transducer sensor errors

Pressure transducers used for water level measurement have certain instrument errors associated with the measurement. The product documentation gives a detail on the magnitude of the error as a water level accuracy or raw pressure accuracy. Water level accuracy is the accuracy of the measurement once the analyst subtracts barometric pressure from the temperature corrected total pressure read by the pressure transducer. A typical value for water level accuracy is 0.05% FS (field scale). Hence if the operation range of the pressure transducer is 0 to 30 ft. and the water level accuracy is 0.05%, the marginal error in the reading is 0.015 feet. Raw pressure accuracy is the accuracy of pressure readings uncorrected for temperature.

3.3.2 Cable length error

The cable used for holding a pressure transducer in a monitoring well may change in length over the monitoring period. Change in a cable length may be due to a stretching of the cable, added length due to a relatively loose clamp used to secure the cable to the well cap, incorrect reinstallation of the pressure transducer during monitoring well sampling events, and/or reading the measurement tape incorrectly while measuring its length. To account for the change in distance between the top of the well casing and the pressure transducer sensor, including the difference between the cable-length-measurement at the beginning and end of the monitoring period and in the overall measurement error.

3.3.3 Vertical well movement error

Monitoring wells may experience a seasonal change to a certain extent. In sub-arctic conditions, freezing and thawing lead to vertical movement over time. The standard operating procedure for groundwater-elevation monitoring for this study site developed by Shannon and Wilson, Inc (a company that is responsible for monitoring and managing the monitoring well network) states that a well is to be re-surveyed after a vertical movement of 0.06 ft. has occurred (Shannon and Wilson, 2013). For the analysis, reported TOC elevation in two consecutive quarterly reports is the same, the marginal error in the well screen's midpoint elevation during the period between the two reporting periods is ±0.06. If the reported TOC elevation is different between two consecutive quarterly reports, the marginal error in the well screen midpoint is equal to the difference between the two TOC elevations. If the well has frost jacked, the marginal error for the well screen midpoint elevation is positive. Thaw subsiding wells are assigned a negative wells screen midpoint elevation marginal error.

3.3.4 Combined error in water level

The random independent errors are associated with water level measurements and pressure transducers (Taylor, 1997; Mandel, 1964):

$$\delta H_i = \sqrt{(\delta PT_i)^2 + (\delta L_i)^2 + (\delta Z_i)^2 + (\delta TOC_i)^2} \qquad (7)$$

In the above equation δH_i is the error in the water level (total head) measured in well where i, δPT_i is the marginal error in the measurement made by the pressure transducer installed below the water line in well i and corrected for barometric pressure (expressed as a pressure head). δL_i is the marginal error in the cable length suspending the pressure transducer in the well, δZ_i is the marginal error in the vertical movement of the well screen midpoint elevation during the

monitoring period, and δTOC_i is the marginal error in the survey measurement of the top of well casing elevation, which is reported to be ±0.01 ft.

Water levels reported from the quarterly reports produced by Aracdis, U.S., Inc. uses Solinst water level meters or an equivalent type of water level meter. Possible errors associated with measuring water level manually using a water level meter includes meter accuracy, error in reading the depth measurement on a ruled tape, error associated with vertical well movement, and error in the survey of the top of casing elevation. The uncertainty for these manually obtained measurements are as follows:

$$\delta H_i = \sqrt{(\delta M_i)^2 + (\delta D_i)^2 + (\delta Z_i)^2 + (\delta TOC_i)^2} \quad (8)$$

δM_i equals the measurement error in the water level meter (0.01 ft.), δD_i equals error in reading the depth measurement on water level sensor ruled tape (0.01 ft.), where the remaining variables are as previously defined.

3.3.5 Propagation of uncertainty into gradient estimates

Two different methods, deterministic and stochastic, are used to account for the uncertainty in the measured total head in each of the four monitoring wells required for the solution of the gradient magnitude and direction determined with Abriola and Pinder's (1982) method. The deterministic approach is only applicable to symmetrical marginal errors. Symmetrical errors cause equal positive or negative uncertainties in the measurement. The marginal error associated with the pressure transducer reading is a good example of a symmetrical error. Vertical movement of a monitoring well due to frost heave or thaw settlement is an example of asymmetrical error. The amount of vertical well movement caused by frost heave in any particular well is most likely not equal to the amount of the well that may settle during the thawing season. The asymmetry of the errors associated with well movement requires a different approach to determine the resulting

uncertainty in the gradient direction and magnitude; the stochastic approach is used for the asymmetrical condition.

The deterministic approach was used to determine the uncertainty in gradient flow and direction from the following general equation for the uncertainty in a multi-variety function whose variables have associated errors (Taylor, 1997):

$$\delta q = \sqrt{\left(\frac{\partial q}{\partial x}\delta x\right)^2 + \cdots + \left(\frac{\partial q}{\partial z}\delta z\right)^2} \tag{9}$$

In the above equation, q is any multivariate function with associated errors in the variables. Applying this equation to Abriola and Pinder's (1982) solution for gradient magnitude is presented above while the uncertainty in the gradient magnitude in the coordinate axis directions is as follows:

$$\delta grad_x = \sqrt{(b_1\delta H_1)^2 + (b_2\delta H_2)^2 + (b_3\delta H_3)^2 + (b_4\delta H_4)^2} \tag{10}$$

$$\delta grad_y = \sqrt{(c_1\delta H_1)^2 + (c_2\delta H_2)^2 + (c_3\delta H_3)^2 + (c_4\delta H_4)^2} \tag{11}$$

$$\delta grad_z = \sqrt{(d_1\delta H_1)^2 + (d_2\delta H_2)^2 + (d_3\delta H_3)^2 + (d_4\delta H_4)^2} \tag{12}$$

$\delta grad_x$, $\delta grad_y$, and $\delta grad_z$ equal the uncertainty in the gradient magnitudes in each of the coordinate directions and H_1, H_2, H_3, and H_4 equal the measured total heads in each monitoring well. Abriola and Pinder (1982) define the constants b, c, and d.

The uncertainty in flow directions in the horizontal plane (θ_{hp}) can be calculated with the following set of equations:

$$\delta\theta_{hp} = \sqrt{\left(\frac{\partial\theta_{hp}}{\partial H_1}\delta H_1\right)^2 + \left(\frac{\partial\theta_{hp}}{\partial H_2}\delta H_2\right)^2 + \left(\frac{\partial\theta_{hp}}{\partial H_3}\delta H_3\right)^2 + \left(\frac{\partial\theta_{hp}}{\partial H_4}\delta H_4\right)^2} \tag{13}$$

$$where, \quad \frac{\partial \theta_{hp}}{\partial H_1} = \frac{\frac{b_1}{grad_y} - \frac{c_1 grad_x}{grad_y{}^2}}{\left(\frac{grad_x}{grad_y}\right)^2 + 1} \tag{14}$$

$\partial\theta_{hp}/\partial H_2$ is similar to substituting b2 and c2 for b1 and c1 in the above equation. Analogous substitutions are made for $\partial\theta_{hp}/\partial H_3$ and $\partial\theta_{hp}/\partial H_4$.

The same procedure is used for determining the uncertainty in the vertical plane flow direction (Θvp). The equations follow:

$$\delta\theta_{vp} = \sqrt{\left(\frac{\partial\theta_{vp}}{\partial H_1}\delta H_1\right)^2 + \left(\frac{\partial\theta_{vp}}{\partial H_2}\delta H_2\right)^2 + \left(\frac{\partial\theta_{vp}}{\partial H_3}\delta H_3\right)^2 + \left(\frac{\partial\theta_{vp}}{\partial H_4}\delta H_4\right)^2} \tag{15}$$

$$where, \quad \frac{\delta\theta_{vp}}{\partial H_1} = \frac{grad_{hp} d_1 - grad_z\left(\frac{grad_x b_1 + grad_y c_1}{grad_{hp}}\right)}{grad_{hp}{}^2 + grad_z{}^2} \tag{16}$$

$grad_{hp}$ equals the gradient magnitude in the horizontal plan, which is equal to $\sqrt{grad_x{}^2 + grad_y{}^2}$. As in the horizontal plan, substitute the appropriate constants (b, c, and d) into Equation 14 to calculate the other three partial derivatives.

3.3.6 Monte Carlo analysis for the errors

The deterministic approach is not applicable to determining the uncertainty in the flow direction and gradient magnitude when the errors result in different positive and negative values, which is the asymmetrical error problem. In these cases, a stochastic approach analysis method by Monte Carlo, which is the repetitive calculation of an analytical or numerical model with different input values derived from probability distributions, is used. Devlin et al., (2007)took this

approach to investigate the effects of measurement error on horizontal gradient estimates. Silliman et al., (2000) used Monte Carlo analysis to examine the effect of measurement errors on the gradient in three dimensions. For this study, a Monte Carlo approach is used to determine the uncertainty in head gradient magnitude and direction with asymmetrical errors in total heads repetitively with Abriola et al., (1982)The method randomly selects each value of total head from uniform probability density function ranging between the upper and lower boundaries of possible total heads for each well determined from Equation 7. Each repetition is referred to as a realization and the compilation of the complete set of realizations an ensemble. The convergence of either the gradient magnitude or direction determines the number of realizations required for an analysis.

To get a better understanding, a simple trail using Group A wells are compared the results from the deterministic and stochastic method. For this comparison, assume a symmetrical and equal error for each well of ±0.02 ft. Table 3.12 Example Deterministic and Stochastic Results for symmetrical marginal errors shows the results from each method.

Table 3.12 Example Deterministic and Stochastic Results for symmetrical marginal errors

Gradient	Deterministic	Stochastic				
		Mean	Standard Deviation	Median	5th Percentile	95th Percentile
Horizontal Magnitude	$9.81 \times 10^{-4} \pm 1.23 \times 10^{-4}$	9.89×10^{-4}	7.07×10^{-5}	9.79×10^{-4}	8.91×10^{-4}	1.12×10^{-3}
Horizontal Direction[1]	343.3° ± 14.47°	344.0°	8.3°	343.5°	330.9°	358.4°
Vertical Magnitude	$1.42 \times 10^{-1} \pm 8.0 \times 10^{-2}$	1.41×10^{-1}	4.48×10^{-2}	1.41×10^{-1}	6.79×10^{-2}	2.16×10^{-1}
Vertical Direction[2]	0.40° ± 0.17°	0.45°	0.17°	0.40	0.29°	0.76°

Comparing results for the gradient magnitudes and directions calculated by both methods for this example with symmetrical errors shows that the two solutions compare somewhat favorably when the marginal errors are compared to the fifth and ninety-fifth percentiles determined from Monte Carlo analysis.

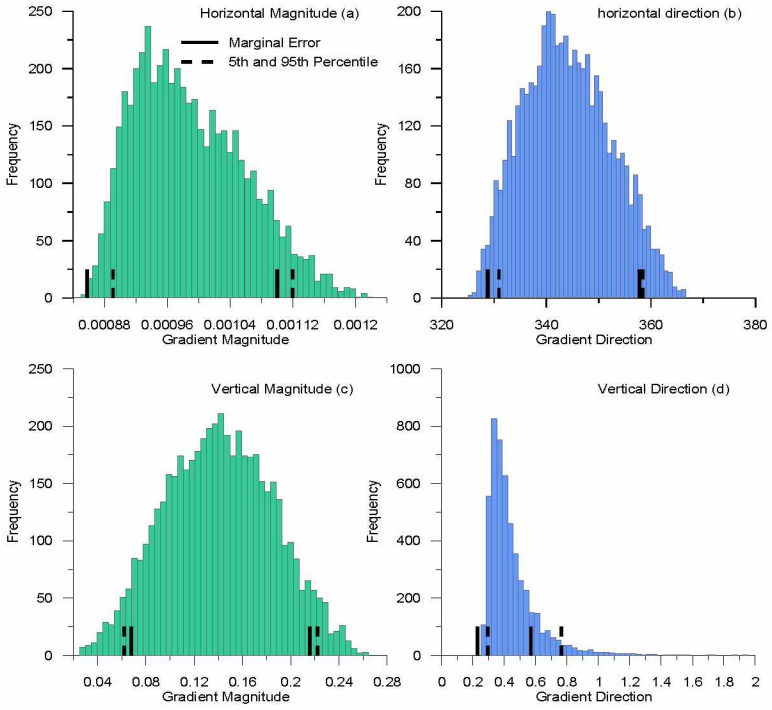

Figure 3.3 Comparison of marginal errors determined by deterministic and stochastic methods

The best comparison occurs when the frequency distribution approaches normality (Gaussian) as panel (c) in Figure 3.3 shows. Frequency distributions that are skewed right (right side is relatively long compared to the left as panel (d) in Figure 3.3 shows) result in an under-prediction of the lower marginal error and an over-prediction of the upper marginal error. This result is expected to owe to the underlying assumption of normality in the marginal error calculation. This result gives the confidence that for symmetrical errors and normally distributed results the Monte Carlo solution provides realistic values of the marginal error in gradient. Moreover, these results give a reasonable percentile for representing the marginal error resulting from asymmetrical errors in water levels.

Each water level measurement has an error of at least ± 0.017 ft. due to errors associated with the instrument used to obtain the water level, reading the measurement, and the survey of the top of casing. Errors are assigned by the vertical movement of the wells by evaluating the TOC

elevation and the date of the TOC survey as discussed before. Table 3.13, Table 3.14, and Table 3.15 show the errors associated with each water level measurement. All the reported well trimming and casing additions are accounted for in the calculations.

Table 3.13 Area A Error in Water Level Measurements for Each Quarter Analyzed

Well depth range	Well ID	Water Level Measurement Error [a] (ft.)					
		1Q14[c]	2Q14	3Q14	4Q15	1Q15	2Q15
Shallow Wells (15 ft. bgs [b])	MW 364-15	-0.017 +0.017	-0.062 +0.062	-0.062 +0.062	-0.062 +0.062	-0.062 +0.062	-0.017 +0.017
	MW 148-15	-0.017 +0.017	-0.017 +0.017	-0.017 +0.017	-0.017 +0.251	-0.017 +0.017	-0.017 +0.026
	MW 359-15	-0.062 +0.062	-0.062 +0.062	-0.062 +0.062	-0.017 +0.017	-0.017 +0.017	-0.017 +0.017
	MW 360-15	-0.062 +0.062	-0.062 +0.062	-0.062 +0.062	-0.020 +0.017	-0.017 +0.017	-0.017 +0.017
Mid Shallow Wells (50-65 ft. bgs)	MW 364-65	-0.017 +0.017	-0.062 +0.062	-0.062 +0.062	-0.017 +0.017	-0.017 +0.017	-0.017 +0.017
	MW 148-55	-0.017 +0.151	-0.017 +0.017	-0.017 +0.017	-0.410 +0.017	-0.017 +0.017	-0.017 +0.017
	MW 359-60	-0.062 +0.062	-0.062 +0.062	-0.062 +0.062	-0.017 +0.035	-0.017 +0.017	-0.017 +0.017
	MW 360-50	-0.062 +0.062	-0.062 +0.062	-0.062 +0.062	-0.017 +0.131	-0.017 +0.017	-0.017 +0.017
Mid Deep Wells (80-90 ft. bgs)	MW 364-90	-0.017 +0.017	-0.062 +0.062	-0.062 +0.062	-0.082 +0.017	-0.062 +0.062	-0.062 +0.062
	MW 148-80	-0.062 +0.062	-0.017 +0.017	-0.17 +0.020	-0.017 +0.017	-0.017 +0.017	-0.017 +0.017
	MW 359-80	-0.062 +0.062	-0.062 +0.062	-0.062 +0.062	-0.017 +0.026	-0.017 +0.017	-0.017 +0.017
	MW 360-80	-0.062 +0.062	-0.062 +0.062	-0.062 +0.062	-0.026 +0.017	-0.017 +0.017	-0.017 +0.017
Deep Wells (150 ft. bgs)	MW 364-150	-0.017 +0.017	-0.062 +0.062	-0.062 +0.062	-0.017 +0.017	-0.062 +0.062	-0.062 +0.062
	MW 148-150	-0.062 +0.062	-0.017 +0.017	-0.017 +0.017	-0.020 +0.017	-0.017 +0.017	-0.017 +0.017
	MW 359-150	-0.062 +0.062	-0.062 +0.062	-0.062 +0.062	-0.020 +0.017	-0.017 +0.017	-0.017 +0.017
	MW 360-150	-0.062 +0.062	-0.062 +0.062	-0.062 +0.062	-0.017 +0.044	-0.017 +0.017	-0.017 +0.017

[a] Calculated based on data obtained from. (ARCADIS, 2014a) (ARCADIS, 2014b) (ARCADIS, 2014c) (ARCADIS, 2014d) (ARCADIS, 2015a), [b] bgs = below ground surface, [c] 1Q14 format represents 1=first Q=Quarter 14= year 2014

Table 3.14 Area B Error in Water Level Measurements for Each Quarter Analyzed

Well depth range	Well ID	Water Level Measurement Error (ft.)					
		1Q14	2Q14	3Q14	4Q15	1Q15	2Q15
Mid Shallow Wells (50-65 ft. bgs)	MW 180-50	-0.017 +0.017	-0.017 +0.017	-0.062 +0.062	-0.062 +0.062	-0.017 +0.017	-0.062 +0.062
	MW 176-50	-0.017	-0.017	-0.062	-0.062	-0.017	-0.062

		+0.017	+0.017	+0.062	+0.062	+0.017	+0.062
	MW 110-65	-0.017 +0.017	-0.017 +0.017	-0.062 +0.062	-0.062 +0.062	-0.017 +0.017	-0.062 +0.062
	MW 336-55	-0.017 +0.017	-0.017 +0.017	-0.062 +0.062	-0.062 +0.062	-0.017 +0.017	-0.062 +0.062
Mid Deep Wells (80-90 ft. bgs)	MW 178-90	-0.062 +0.062	-0.062 +0.062	-0.062 +0.062	-0.062 +0.062	-0.017 +0.017	-0.062 +0.062
	MW 175-90	-0.017 +0.017	-0.017 +0.017	-0.017 +0.017	-0.017 +0.017	-0.017 +0.017	-0.017 +0.017
	MW 174-90	-0.017 +0.017	-0.017 +0.017	-0.017 +0.017	-0.017 +0.017	-0.017 +0.017	-0.017 +0.017
	MW 176-90	-0.062 +0.062	-0.062 +0.062	-0.062 +0.062	-0.062 +0.062	-0.017 +0.017	-0.062 +0.062

[a] Calculated based on data obtained from. (ARCADIS, 2014a) (ARCADIS, 2014b) (ARCADIS, 2014c) (ARCADIS, 2014d) (ARCADIS, 2015a), [b] bgs = below ground surface, [c] 1Q14 format represents 1=first Q=Quarter 14= year 2014

Table 3.15 Area C Error in Water Level Measurements for Each Quarter Analyzed

Well depth range	Well ID	Water Level Measurement Error [a] (ft.)					
		1Q14[c]	2Q14	3Q14	4Q15	1Q15	2Q15
Shallow Wells (15 ft. bgs [b])	MW-306-15	-0.017 +0.017	-0.020 +0.017	-0.017 +0.017	-0.017 +0.017	-0.017 +0.017	-0.017 +0.017
	MW-173-15	-0.062 +0.062	-0.017 +0.017	-0.062 +0.062	-0.062 +0.062	-0.062 +0.062	-0.062 +0.062
	MW-334-15	-0.017 +0.017	-0.035 +0.017	-0.017 +0.020	-0.017 +0.026	-0.017 +0.026	-0.017 +0.017
	MW-304-15	-0.017 +0.017	-0.017 +0.017	-0.017 +0.017	-0.017 +0.035	-0.017 +0.020	-0.017 +0.017
Mid Deep Wells (70-90 ft. bgs)	MW-306-70	-0.062 +0.062	-0.017 +0.017	-0.062 +0.062	-0.017 +0.020	-0.017 +0.017	-0.017 +0.017
	MW-144-90	-0.062 +0.062	-0.017 +0.026	-0.062 +0.062	-0.062 +0.062	-0.062 +0.062	-0.062 +0.062
	MW-334-85	-0.062 +0.062	-0.017 +0.020	-0.017 +0.017	-0.020 +0.017	-0.020 +0.017	-0.017 +0.044
	MW-304-80	-0.017 +0.017	-0.017 +0.026	-0.017 +0.020	-0.017 +0.017	-0.017 +0.020	-0.020 +0.017
Deep Wells (150 ft. bgs)	MW-306-150	-0.017 +0.017	-0.017 +0.017	-0.017 +0.017	-0.017 +0.020	-0.017 +0.017	-0.020 +0.017
	MW-173-150	-0.062 +0.062	-0.017 +0.062	-0.062 +0.062	-0.062 +0.062	-0.062 +0.062	-0.062 +0.062
	MW-307-150	-0.017 +0.017	-0.017 +0.020	-0.020 +0.017	-0.020 +0.017	-0.017 +0.017	-0.017 +0.026
	MW-304-150	-0.017 +0.017	-0.017 +0.020	-0.020 +0.017	-0.017 +0.020	-0.017 +0.026	-0.020 +0.017

[a] Calculated based on data obtained from. (ARCADIS, 2014a) (ARCADIS, 2014b) (ARCADIS, 2014c) (ARCADIS, 2014d) (ARCADIS, 2015a), [b] bgs = below ground surface, [c] 1Q14 format represents 1=first Q=Quarter 14= year 2014

Table 3.16 Continuous Area Error in Water Level Measurements for Each Quarter Analyzed

Well depth range	Well ID	Water Level Measurement Error [a] (ft)				
		4Q14[c]	1Q15	2Q15	3Q15	4Q15
Shallow Wells (15 ft bgs [b])	MW 148-15	-0.017 +0.251	-0.017 +0.017	-0.017 +0.026	-0.062 +0.062	-0.400 +0.017
	MW 304-15	-0.017 +0.035	-0.017 +0.020	-0.017 +0.017	-0.151 +0.017	-0.017 +0.020
	MW 364-15	-0.062 +0.062	-0.062 +0.062	-0.017 +0.017	-0.920 +0.017	-0.017 +0.017
	MW 309-15	-0.062 +0.062	-0.062 +0.062	-0.062 +0.062	-0.017 +0.020	-0.281 +0.017
Mid Shallow Wells (40-70 ft bgs)	MW 358-40	-0.017 +0.017	-0.062 +0.062	-0.017 +0.020	-0.035 +0.017	-0.017 +0.026
	MW 309-66	-0.026 +0.017	-0.062 +0.062	-0.020 +0.017	-0.121 +0.017	-0.026 +0.017
	MW 306-70	-0.020 +0.017	-0.062 +0.062	-0.017 +0.017	-0.017 +0.017	-0.017 +0.020
	MW 148-55	-0.017 +0.072	-0.062 +0.320	-0.310 +0.017	-0.440 +0.062	-0.017 +0.017
Deep Wells (150 ft bgs)	MW 306-150	-0.017 +0.020	-0.017 +0.017	-0.020 +0.017	-0.017 +0.017	-0.017 +0.020
	MW 360-150	-0.017 +0.044	-0.017 +0.017	-0.017 +0.017	-0.017 +0.017	-0.020 +0.017
	MW 358-150	-0.017 +0.017	-0.072 +0.062	-0.017 +0.017	-0.035 +0.017	-0.017 +0.035
	MW 304-150	-0.017 +0.020	-0.017 +0.026	-0.020 +0.017	-0.026 +0.017	-0.017 +0.026

[a] Calculated based on data obtained from. (ARCADIS, 2014a)(ARCADIS, 2014b)(ARCADIS, 2014c)(ARCADIS, 2014d)(ARCADIS, 2015a), [b] bgs = below ground surface, [c] 4Q14 format represents 4=fourth Q=Quarter 14= year 2014

Using the errors in the tables above, the best estimate of a flow gradient and direction for discrete and continuous well clusters is made, which is discussed in the results chapter.

Chapter 4 Results

The results provided in the methods section are discussed and explained in this chapter. As discussed in the methods section, the data is divided into the Discrete analysis, which is a moment in time measurements, and Continous analysis, which involves a continuous set of data.

4.1 Gradient Magnitudes and Flow Direction for Discrete Analysis

4.1.1 Area A wells

Table 4.1 shows the results from Monte Carlo analyses of the gradient magnitudes and flow direction in the horizontal and vertical planes using the data provided in Chapter 3 for Area A wells. Median values of the horizontal gradient magnitudes range from a low of approximately 9×10^{-5} to a high of 3×10^{-3} m/m. Directions in the horizontal plane are measured clockwise from North (0°). Using this convention, the Monte Carlo results show that the median direction in the horizontal plane ranges between northwest to northeast.

In the vertical plane, the median values of the gradient magnitudes range over three-orders of magnitude from approximately 10^{-3} to 1.7 m/m. Vertical plane flow direction results are presented where 0° is the vertically upward flow and 180° is the vertically downward flow. As Table 4.1 shows, the marginal errors in vertical flow direction are large for some of the measurement periods. Results at the shallow water table (15 ft.) show a downward flow direction with no uncertainty or upward with a possibility of downward flow taking into consideration marginal error.

A comparison between vertical flow direction and trend in water level may provide an explanation for the variability in the vertical flow direction, especially at the water table. For this

comparison water levels measured in MW 148-15 are to be representative of the water table elevation in the area of Group A. Owing to the lack of continuous water level measurements spanning the range of dates in our analyses, trends in the Tanana River gauge height for time periods not included in the continuous water levels measured in Group A wells. To use the Tanana River gauge height in this analysis, the lag time between a change in water elevation in the river and the associated change in water levels measured in MW 148-15 must be determined. A comparison of the two water levels, shown in Figure 4.1, indicates that there is an approximately two to four-day lag time between changes in river gauge height and corresponding changes in water level in the Group A well location. Taking this lag time into consideration, Figure 4.2 shows the trends in water levels for seven days prior to the water level measurement date for each individual quarter. Comparing these trends to the vertical direction of flow at the water table (Table 4.1) suggests that a rising water level results in upward flow at the water table and a falling water level results in downward flow at the water table. This flow pattern makes intuitive sense. Characterization of the aquifer indicates that relatively lower conductivity soils overlay soils with greater hydraulic conductivities. Hence, vertical flow patterns distant from a surface water source in aquifers with layered soils tend to be upward as water recharges aquifers and downwards as water tables fall.

At the mid-shallow depth (50 to 65 ft.), vertical flow is constantly upward with no possibility of downward flow. During periods when the vertical flow direction is downward at the water table, a converging flow pattern that exists between directions of flow at the water table and at the 50-65 ft. BGS (below ground surface) depth in the area of Group A wells. This flow pattern is due to groundwater above the vertical groundwater divide routing into the supra-permafrost portion of the aquifer as hypothetically shown in Figure 1.2.

At mid-deep (80 to 90 ft.), depth level is either down with no possibility of upward flow or upward with a possibility of downward flow. At the deep level (150 ft.), the flow is either upward with no possibility of downward flow, upward with a possibility of downward flow, or downward with a possibility upward flow. Reasons for the changing flow direction at these depths are currently not known.

Histograms of the vertical flow direction generated by the Monte Carlo analysis are shown in Figure 4.3 and Figure 4.4. Several of these histograms show the Monte Carlo analysis results in a bimodal distribution of vertical flow directions. Silliman et al., (2000) showed a similar result in a study on the effect of the error on the hydraulic gradient in three dimensions. They attribute the resulting bimodal distribution in their study to the close vertical spacing of the wells screens for each of the four wells.

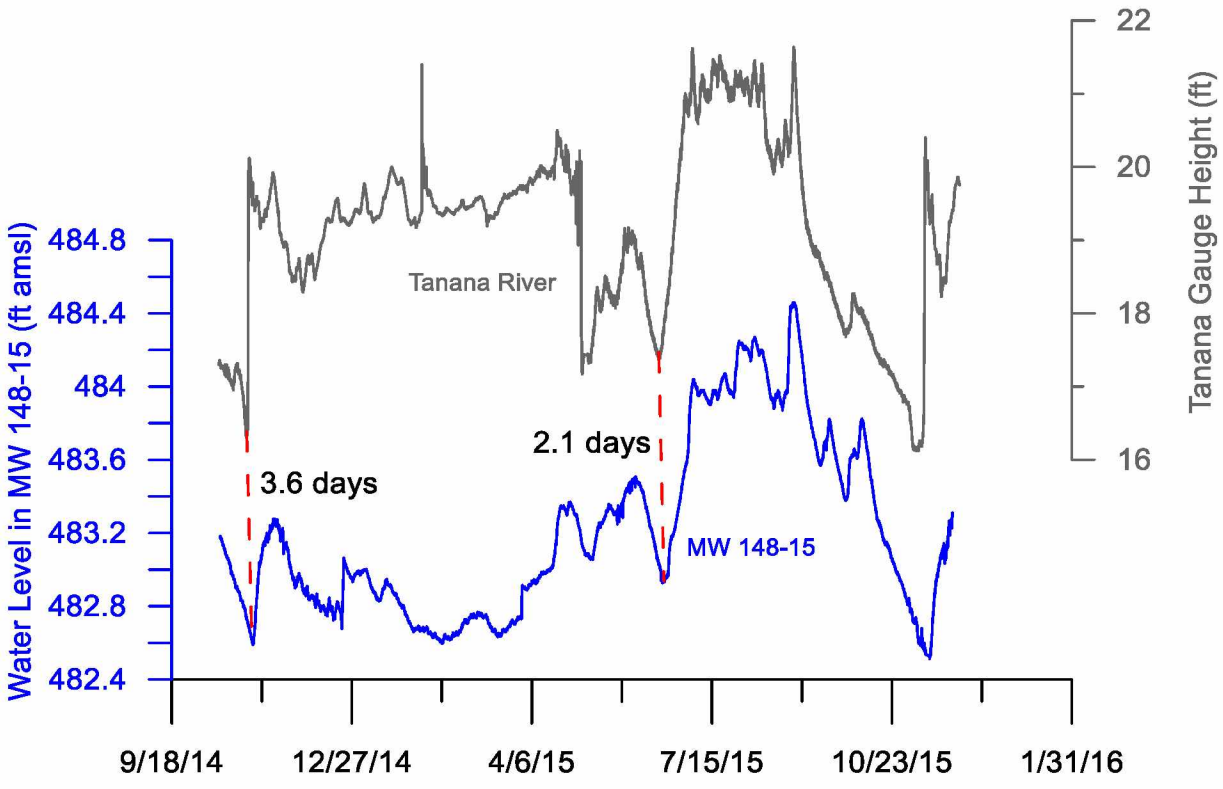

Figure 4.1 Comparison between water level elevation in MW 148-15 versus Tanana Gauge Height

To determine an approximate lag time between changes in the Tanana stage and groundwater levels in Group A Wells.

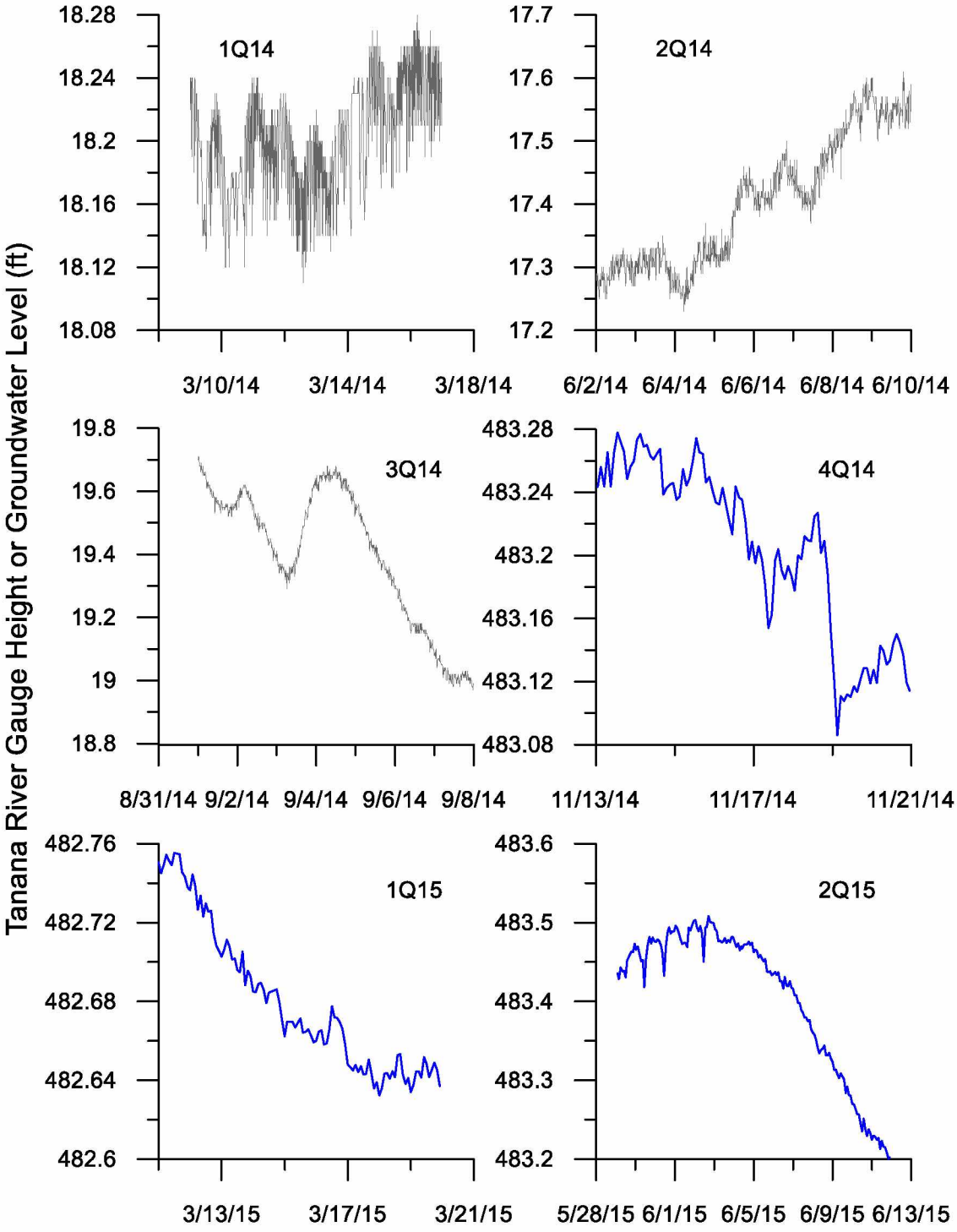

Figure 4.2 Water level trends for an approximate seven-day period prior to the date groundwater level

These measurements were used in determining vertical gradient. Gray trend lines correspond to the Tanana gauge height and blue trend lines correspond to water levels in MW 148-15.

Table 4.1 Area A Wells – Gradient Magnitudes and Flow Direction

Date (Quarter)	Depth (ft. bgs)	Horizontal		Vertical	
		Magnitude (10^{-3}) Median (5^{th}/95^{th} %iles)	Flow Direction Median (5^{th}/95^{th} %iles)	Magnitude Median (5^{th}/95^{th} %iles)	Flow Direction Median (5^{th}/95^{th} %iles)
March 18-19, 2014 (1Q14)	Water Table (15)	1.09(0.94/1.47)	338° (315°/14°)	0.17 (0.016/0.42)	0.4° (0.2°/179°)
	Mid (50-65)	0.86 (0.74/0.98)	10° (353°/27°)	0.0080 (0.0024/0.014)	6° (4°/18°)
	Mid-Deep (80-90)	0.72 (0.56/0.86)	337° (305°/6°)	0.017 (0.0031/0.031)	178° (165°/179°)
	Deep (150)	0.85 (0.60/1.48)	355° (331°/55°)	0.074 (0.0064/0.19)	1° (0.4°/180°)
June 11, 2014 (2Q14)	Water Table (15)	3.04 (0.86/6.80)	322° (313°/64°)	2.14 (0.18/5.36)	0.1° (0.1°/180°)
	Mid (50-65)	0.86 (0.71/1.04)	26° (15°/35°)	0.0071 (0.0013/0.013)	7° (4°/34°)
	Mid-Deep (80-90)	0.77 (0.66/0.86)	330° (302°/358°)	0.017 (0.0026/0.032)	177° (156°/179°)
	Deep (150)	0.90 (0.68/1.20)	43° (354°/82°)	0.095 (0.086/0.24)	179° (1°/180°)
Sept. 9, 2014 (3Q14)	Water Table (15)	1.32 (0.76/2.52)	300° (281°/14°)	1.68 (0.29/3.10)	180° (180°/180°)
	Mid (50-65)	0.98 (0.84/1.15)	292° (284°/302°)	0.027 (0.021/0.033)	2° (1°/3°)
	Mid-Deep (80-90)	0.086 (0.075/0.099)	320° (298°/347°)	0.0097 (0.00083/0.025)	5° (2°/170°)
	Deep (150)	1.34 (0.60/2.10)	310° (304°/323°)	0.14 (0.011/0.27)	0.7° (0.4°/179°)
Nov. 20-21, 2014 (4Q14)	Water Table (15)	1.43 (1.11/1.96)	330° (313°/1°)	0.55 (0.069/1.07)	180° (171°/180°)
	Mid (50-65)	1.10 (0.74/1.57)	326° (312°/354°)	0.014 (0.0089/0.020)	4° (2°/8°)
	Mid-Deep (80-90)	0.82 (0.78/0.87)	327° (319°/337°)	0.0034 (0.0003/0.0095)	163° (11°/175°)
	Deep (150)	1.23 (0.92/1.55)	323° (318°/332°)	0.090 (0.022/0.16)	0.8° (0.6°/2°)
March 18-19, 2014 (1Q15)	Water Table (15)	1.78 (1.49/2.07)	311° (306°/318°)	0.86 (0.66/1.08)	180° (180°/180°)
	Mid (50-65)	0.81 (0.77/0.84)	344° (340°/350°)	0.0042 (0.0026/0.0059_	11° (8°/17°)
	Mid-Deep (80-90)	0.78 (0.74/0.82)	333° (326°/341°)	0.0059 (0.0006/0.013)	172° (39°/177°)
	Deep (150)	0.80 (0.57/1.14)	330° (316°/358°)	0.028 (0.0027/0.077)	177° (2°/180°)
June 4-11, 2014 (2Q15)	Water Table (15)	0.93 (0.87/0.98)	29° (17°/39°)	0.29 (0.20/0.37)	0.2° (0.1°/0.3°)
	Mid (50-65)	0.93 (0.90/0.97)	340° (336°/344°)	0.0033 (0.0016/0.0049)	16° (11°/30°)
	Mid-Deep (80-90)	0.93 (0.88/0.98)	325° (319°/332°)	0.010 (0.0030/0.017)	175° (163°/177°)
	Deep (150)	0.069 (0.059/0.093)	353° (329°/31°)	0.063 (0.0073/0.13)	179° (41°/180°)

Bgs= below ground surface, 1Q14 format represents 1=first Q=Quarter 14= year 2014, %iles= percentiles

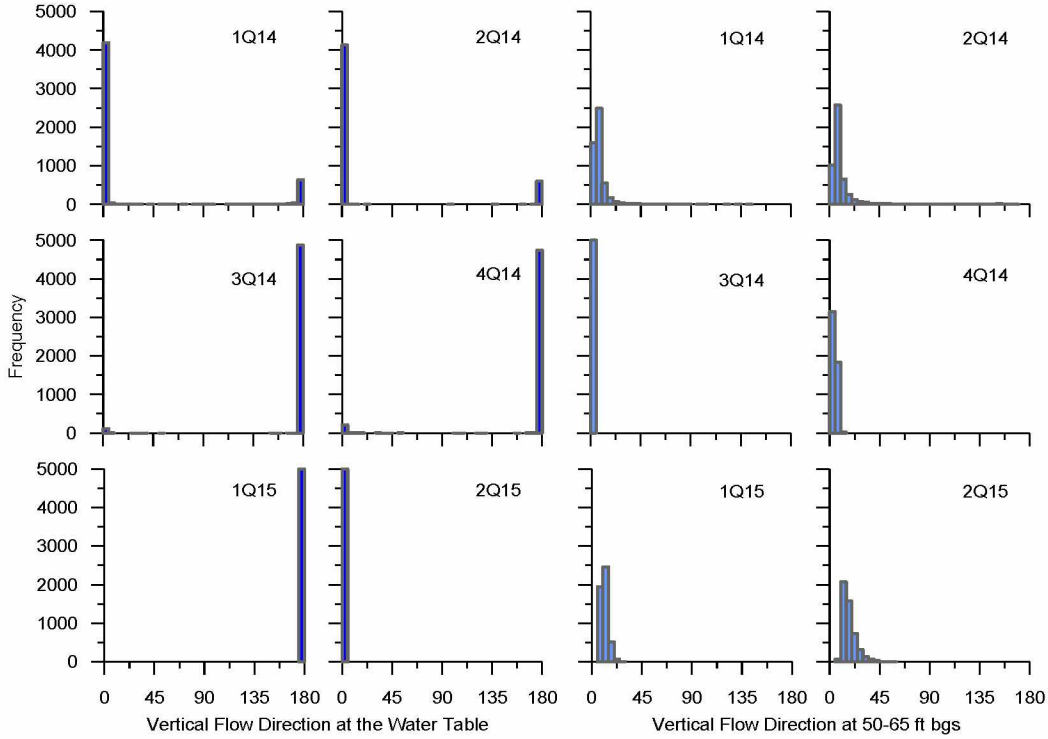

Figure 4.3 Probability distribution of vertical flow direction for Area A water table and mid shallow wells

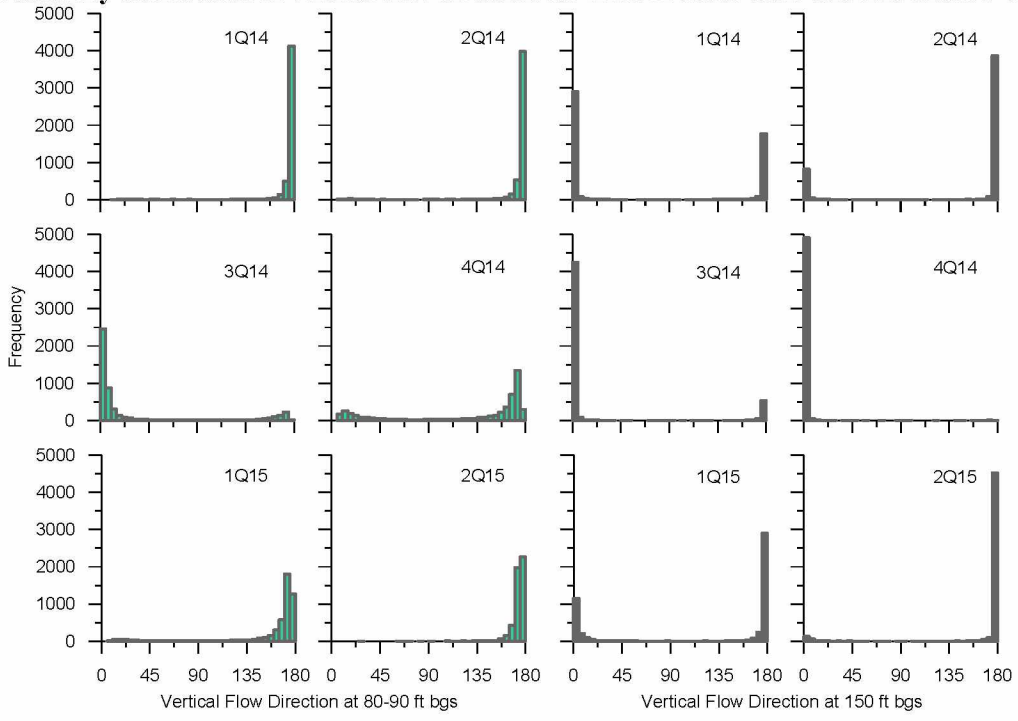

Figure 4.4 Probability distribution of vertical flow direction for Area A mid-deep and deep wells

4.1.2 Area B wells

The location of Area B is shown in Figure 4.5. Data mentioned in Table 3.6 shows the frozen wells in the monitoring period for Area B, so the analysis is limited to unfrozen wells and well depths deep enough not to be influenced by groundwater capture pumping wells in the area. The results for flow direction and gradient magnitude determined for the Area B in Table 4.2 and Figure 4.6 show variability similar to those found in Area A. The major contrast between these two areas is the median flow direction at mid-shallow depth (50-65 ft bgs). Analysis of the vertical flow direction in Area A shows vertical flow direction at the mid-shallow depth is directed upward for all six quarters analyzed. However, in Area B, gradient analysis results show a downward flow direction for Area B wells. With only two-quarters of data (3Q14 and 4Q14), it is difficult to provide a reason for the difference between the two well areas. However, it is possible that a small zone of permafrost, which exists in the flood plain talik as demonstrated by the geophysical surveys (Figure 2.2 and Figure 2.3) is causing a downward flow pattern as groundwater routes around the frozen soil. Vertical groundwater flow directions at the mid-deep depths range between upward and downward similar to the flow patterns determined in the Area A wells. A close examination of the results from Area B indicates that the two periods of upward flow at this depth occurred in June (June 11, 2014, and June 4-11, 2015). The cause of this flow pattern is currently unknown.

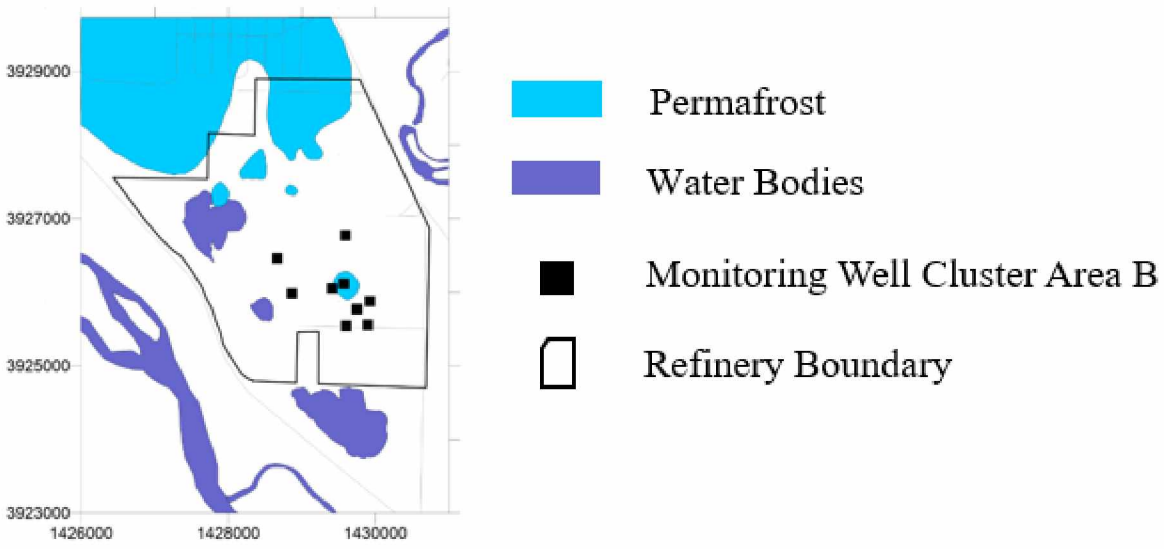

Figure 4.5 Location of Area B

Table 4.2 Area B Wells – Gradient Magnitudes and Flow Direction

Date (Quarter)	Depth (ft. bgs)	Horizontal		Vertical	
		Magnitude (10^{-3}) Median (5^{th}/95^{th} %iles)	Direction Median (5^{th}/95^{th} %iles)	Magnitude Median (5^{th}/95^{th} %iles)	Direction Median (5^{th}/95^{th} %iles)
March 18-19, 2014 (1Q14)	Mid shallow (50-65)	Frozen wells			
	Mid Depth (80-90)	1.22 (1.04/1.88)	359° (318°/56°)	0.23 (0.023/0.61)	179° (0.3°/180°)
June 11, 2014 (2Q14)	Mid shallow (50-65)	Frozen wells			
	Mid deep (80-90)	1.39 (1.27/1.51)	285° (284°/285°)	5.38 (4.92/5.84)	0.1° (0.1°/0.1°)
Sept. 9, 2014 (3Q14)	Mid shallow (50-65)	1.81 (0.89/3.20)	356° (308°/369°)	0.025 (0.0027/0.056)	176° (12°/177°)
	Mid deep (80-90)	1.19 (0.95/2.05)	338° (311°/40°)	0.20 (0.018/0.52)	177° (0.3°/180°)
Nov. 20-21, 2014 (4Q14)	Mid shallow (50-65)	1.99 (0.91/3.34)	359° (317°/10°)	0.027 (0.0032/0.057)	176° (22°/177°)
	Mid deep (80-90)	1.29 (1.14/1.83)	4° (324°/54°)	0.24 (0.025/0.67)	180° (0.4°/180°)
June 4-11, 2014 (2Q15)	Mid shallow (50-65)	Frozen wells			
	Mid deep (80-90)	2.14 (1.27/3.25)	310° (300°/336°)	0.51 (0.076/0.98)	0.2° (0.2°/1°)

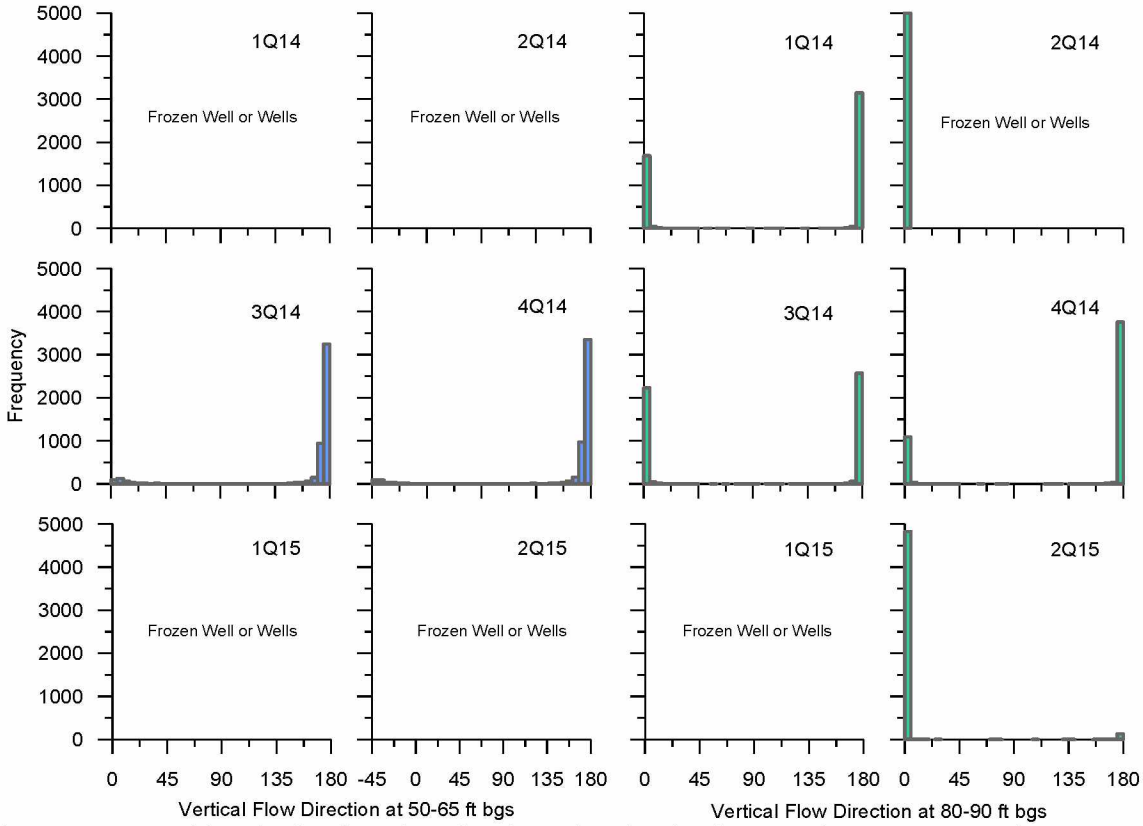

Figure 4.6 Probability distribution of vertical flow direction for Area B mid-shallow and mid deep wells

4.1.3 Area C wells

Table 4.3and Figure 4.7 show the Monte Carlo results of gradient and magnitude and flow direction in Area C. Contrary to Area A and B results, the median vertical gradients in Area C well area are nearly all consistently upwards for the three depths analyzed with minimal marginal errors (Table 3.15). The configuration of permafrost in Area C wells may be causing a different flow pattern in comparison to the flow pattern in the Area A and B well areas.

Table 4.3 Area C Wells – Gradient Magnitudes and Flow Direction

Date (Quarter)	Depth (ft. bgs)	Horizontal		Vertical	
		Magnitude (10^{-3}) Median (5^{th}/95^{th} %iles)	Flow Direction Median (5^{th}/95^{th} %iles)	Magnitude Median (5^{th}/95^{th} %iles)	Flow Direction Median (5^{th}/95^{th} %iles)
March 18-19, 2014 (1Q14)	Water Table (15)	Frozen	Frozen	Frozen	Frozen
	Mid-Deep (70-90)	0.71 (0.82/0.59)	348° (342°/354°)	0.00013 (0.0062/+0.006)	79° (6°/172°)
	Deep (150)	0.99 (1.12/0.86)	27° (344°/409°)	0.71 (1.65/0.22)	0.09° (0.06°/179°)
June 11, 2014 (2Q14)	Water Table (15)	0.38 (0.41/0.35)	315° (311°/318°)	0.07 (0.08/0.05)	0.5° (0.4°/0.6°)
	Mid-Deep (70-90)	0.71 (0.75/0.68)	345° (342°/348°)	0.0023(0.0044/0.0002)	18° (9°/75°)
	Deep (150)	1.16 (1.27/1.06)	57° (408°/422°)	2.41 (3.14/1.69)	0.05° (0.049°/0.054°)
Sept. 9, 2014 (3Q14)	Water Table (15)	0.24 (0.26/0.22)	291° (288°/295°)	0.09 (0.11/0.08)	0.4° (0.4°/0.5°)
	Mid-Deep (70-90)	0.68 (0.75/0.62)	339° (332°/345°)	0.007 (0.012/0.0017)	6° (3°/24°)
	Deep (150)	1.26 (1.37/1.16)	60° (413°/424°)	3.04 (3.85/2.23)	0.048° (0.04°/0.049°)
Nov. 20-21, 2014 (4Q14)	Water Table (15)	0.43 (0.45/0.40)	318° (313°/324°)	0.07 (0.09/0.06)	0.5° (0.4°/0.6°)
	Mid-Deep (70-90)	0.69 (0.75/0.63)	348° (343°/352°)	0.007 (0.011/0.003)	6° (3°/14°)
	Deep (150)	1.18 (1.29/1.07)	61° (411°/427°)	2.84 (3.84/1.84)	0.05° (0.048°/0.053°)
March 18-19, 2014 (1Q15)	Water Table (15)	0.43 (0.45/0.40)	318° (313°/324°)	0.07 (0.09/0.06)	0.5° (0.4°/0.6°)
	Mid-Deep (70-90)	0.67 (0.73/0.60)	346° (341°/351°)	0.004 (0.009/0.0008)	8° (4°/42°)
	Deep (150)	Frozen	Frozen	Frozen	Frozen
June 4-11, 2014 (2Q15)	Water Table (15)	0.33 (0.36/0.30)	313° (307°/320°)	0.07 (0.09/0.05)	0.4° (0.4°/0.5°)
	Mid-Deep (70-90)	0.77 (0.85/0.70)	348° (343°/351°)	+0.0002 (0.004/+0.005)	108° (10°/170°)
	Deep (150)	1.18 (1.35/1.02)	52° (388°/422°)	2.01 (3.18/0.84)	0.055° (0.05°/0.08°)

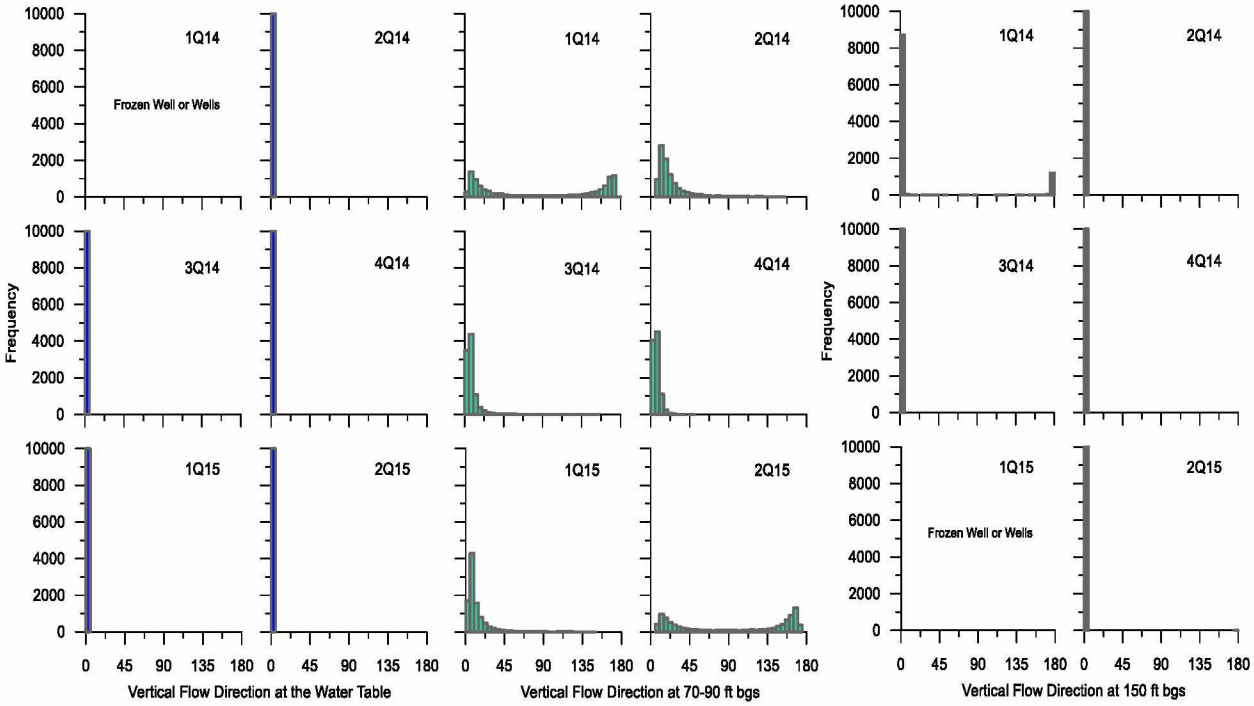

Figure 4.7 Probability distribution of vertical flow direction for Area C

4.2 Continuous Area Wells

The location of Continuous area wells is shown in Figure 3.2. Using the data from Table 3.10, Table 3.11, and

Table 3.16, the gradient magnitudes and flow directions for the period of October 2014 through December 2015 have been analyzed.

To understand the vertical flow variability, the water levels from the shallow wells are compared with trends in the Tanana River gauge height for the selected time periods, as it is the recharge for groundwater in the study area. The lag time between a change in water elevation in the river and the associated change in groundwater levels in the area determined are shown in Figure 4.1.

4.2.1 Shallow wells

The water levels of wells used for shallow depth (15 ft.) are shown in Figure 4.8. The water level elevations on the left side of the y-axis for the four wells vary between 482.5 to 485.5 feet, which shows how closely it changes in the vertical profile even though they have large spatial variability. When the water levels are compared with the Tanana stage height on the right side of the y-axis, the lag time is observed with a reasonable similarity in the overall trend as shown in Figure 4.1. The results of vertical flow direction are shown in Figure 4.10, with the median of error plotted within error bounds of 5^{th} and 95^{th} percentiles. The flow varies between 0.1^0 and 0.25^0 over the monitoring period, which is always upward. To check the major influencing well for the shallow well flow direction changes, Figure 4.9 shows the errors in water levels of individual wells. Due to the marginal error in MW 364-15, the vertical flow direction had a minor shift during the end of June until the end of September 2015. Comparing the vertical flow to the Tanana stage, as the river resides during the winter months, vertical flow direction shows an increase in trend. Tanana may be gaining groundwater during these months.

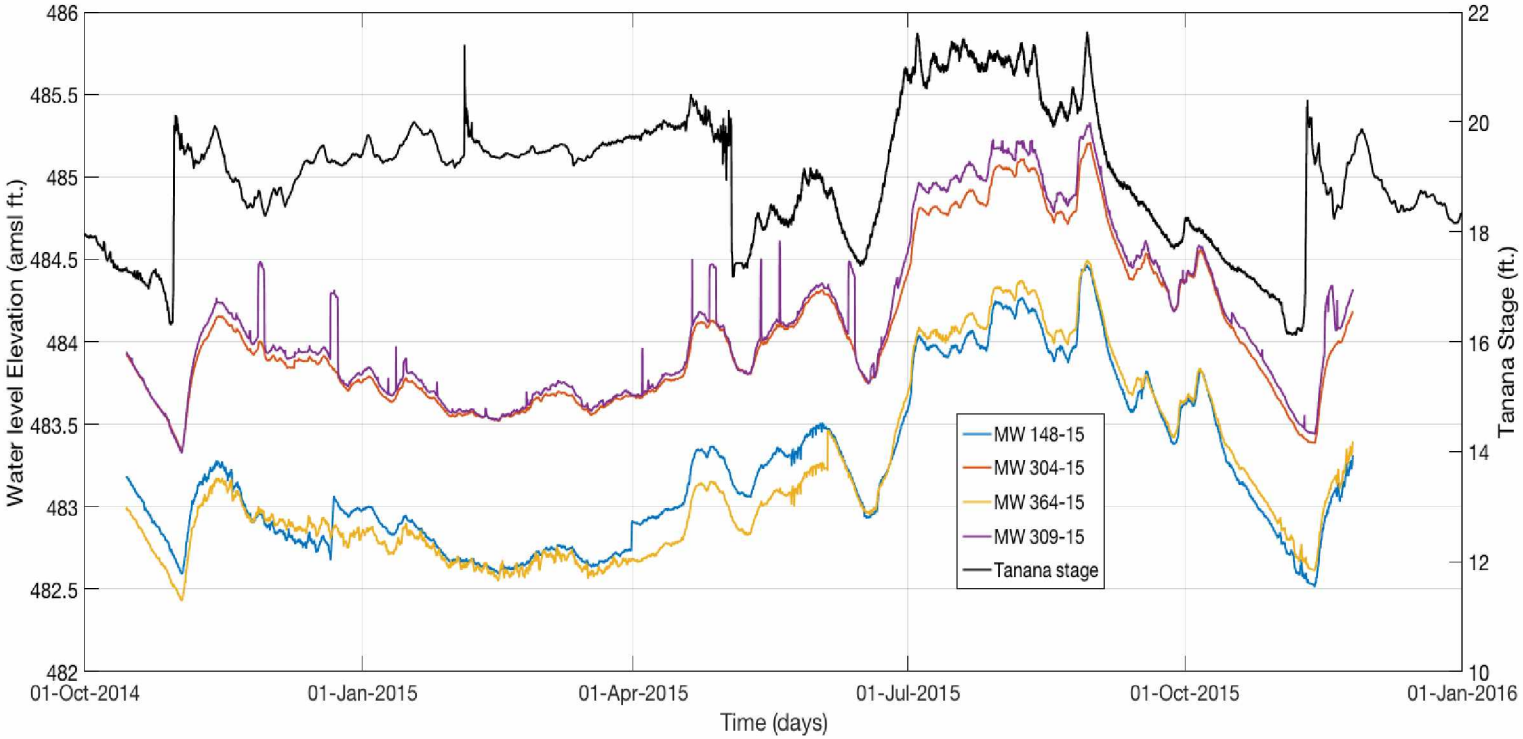

Figure 4.8 Water level elevations for shallow (15 ft.) wells in Continuous Area

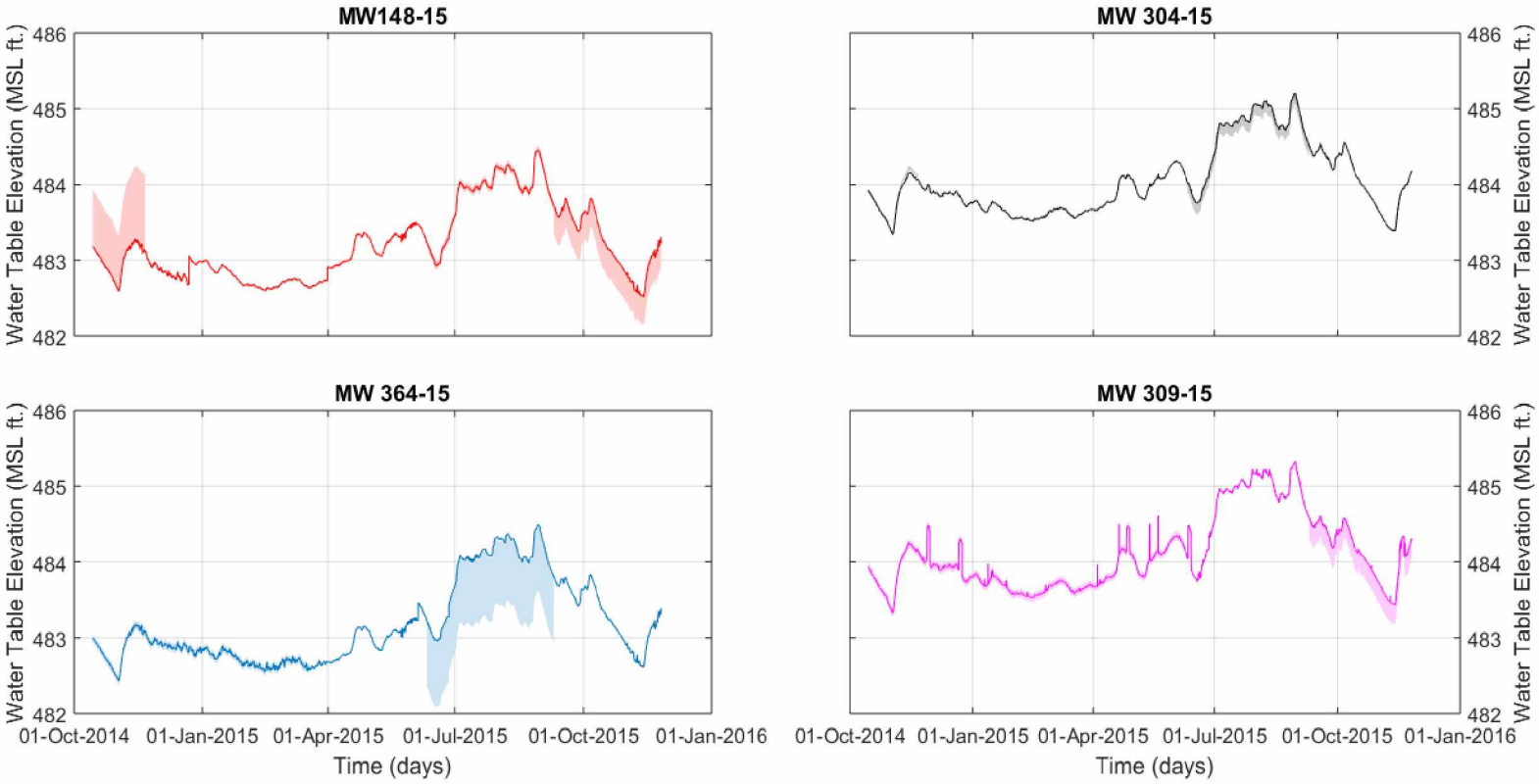

Figure 4.9 Errors in water level elevations for shallow (15 ft.) wells in Continuous Area

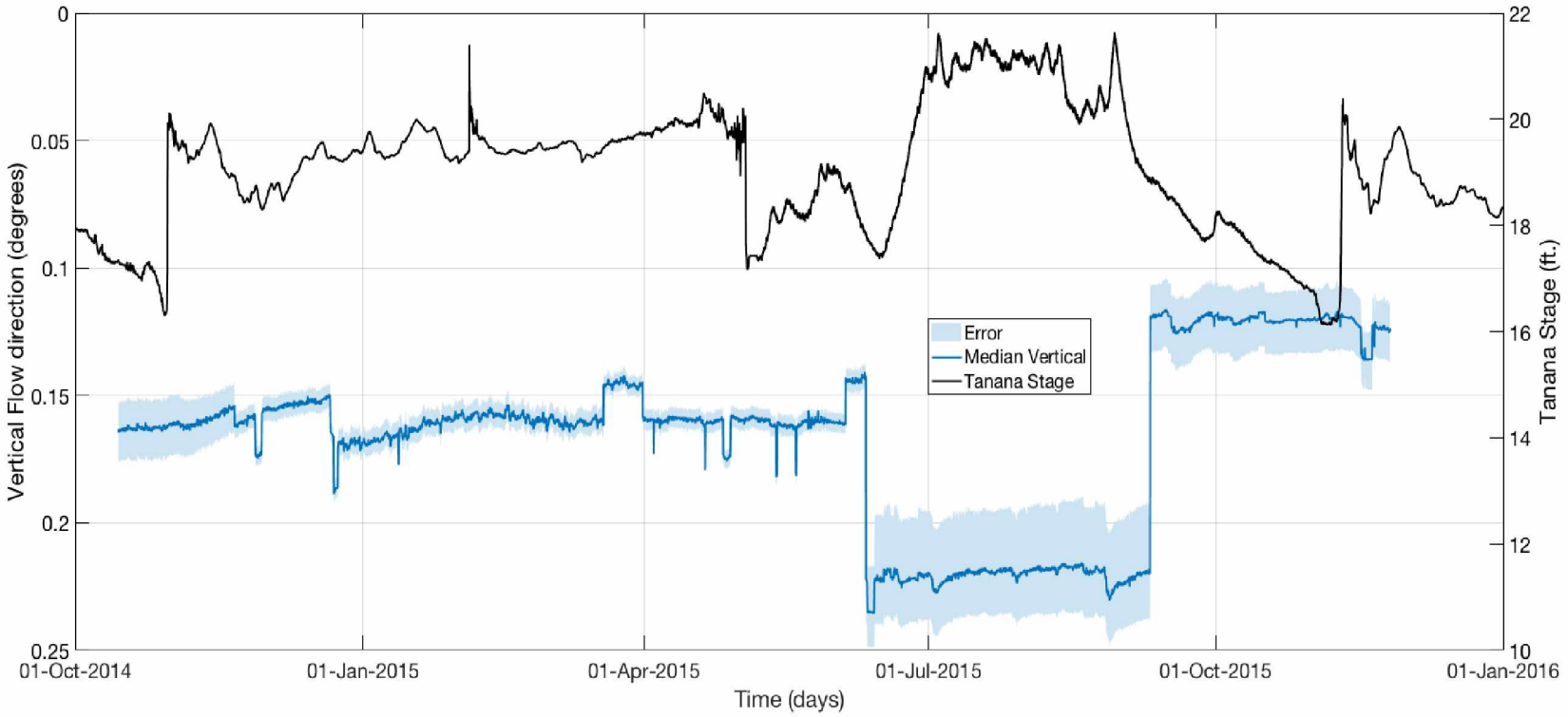

Figure 4.10 Vertical flow direction with median for shallow (15 ft.) wells in Continuous Area

4.2.2 Mid-shallow wells

The water levels for the mid-shallow wells (40 to 70ft.) are shown in Figure 4.11 and the errors associated with individual wells are shown in Figure 4.12. The median of vertical flow direction calculated with the marginal error and error bounds of the 5^{th} and 95^{th} percentiles are shown in Figure 4.13. The marginal error in MW 148-55 is considerably high shown in comparison to the other three wells as shown in Figure 4.12. This high marginal error is one of the reasons for variation in error bounds of the 5^{th} and 95^{th} percentiles from upward to downward. Groundwater flow direction during this monitoring period shows the sensitivity to change in the vertical direction. In Area A and B wells, the existence of a vertical groundwater divide is located between 65 and 90 ft. bgs, which is a short distance below the top of permafrost. The fluctuating vertical flow direction in the continuously monitored mid depth wells is most likely a result of fluctuations in the depth of the vertical flow divide.

4.2.3 Deep wells

The water levels plotted for deep wells are shown in Figure 4.14 while the errors in individual water levels are shown in Figure 4.14. The median of vertical flow direction with error bounds between the 5^{th} and 95^{th} percentiles are shown in Figure 4.16. The flow direction is downward close to 179^0 throughout the monitoring period with a very little variability in the median, even though the 5^{th} percentile has a range close to 0^0 upward.

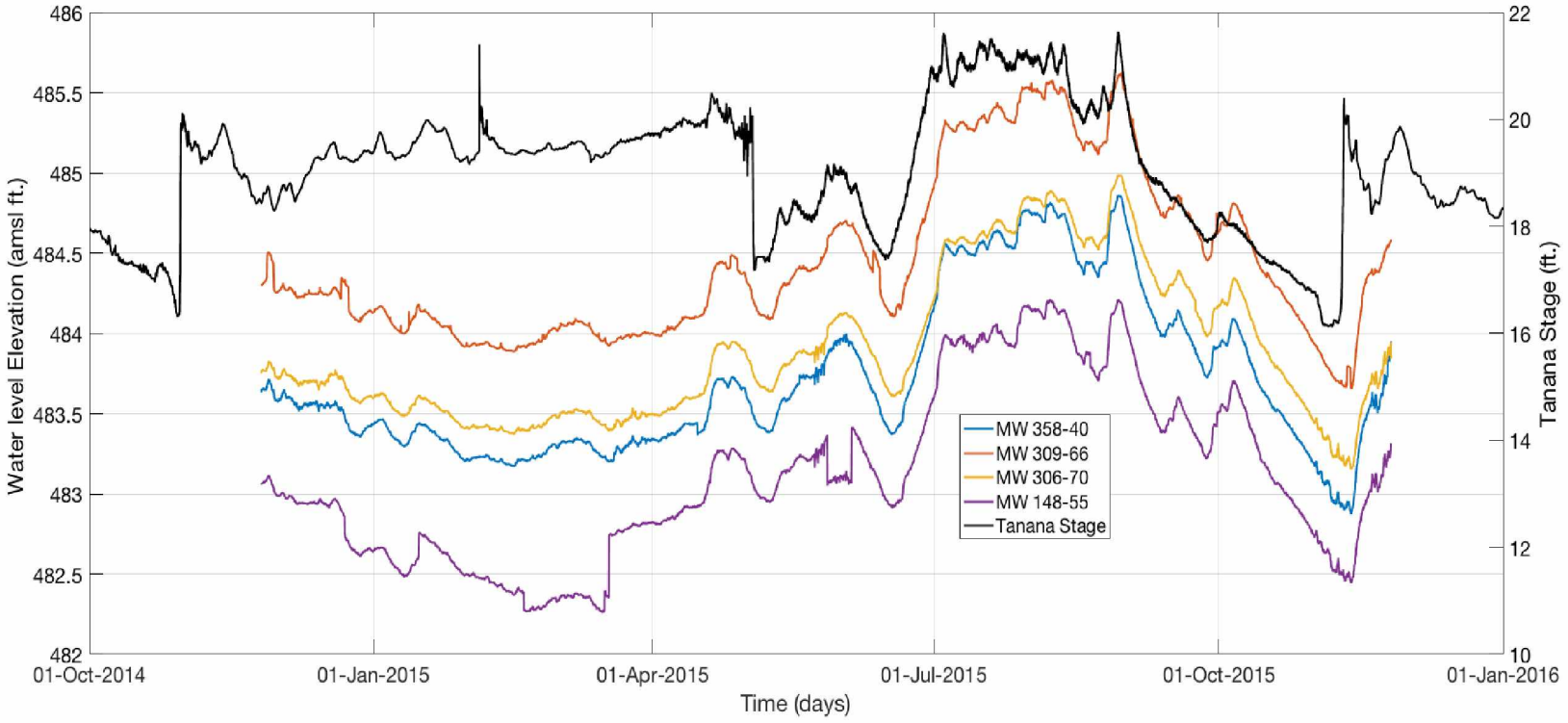

Figure 4.11 Water level Elevations for mid-shallow (40 to 70 ft.) wells in Continuous Area

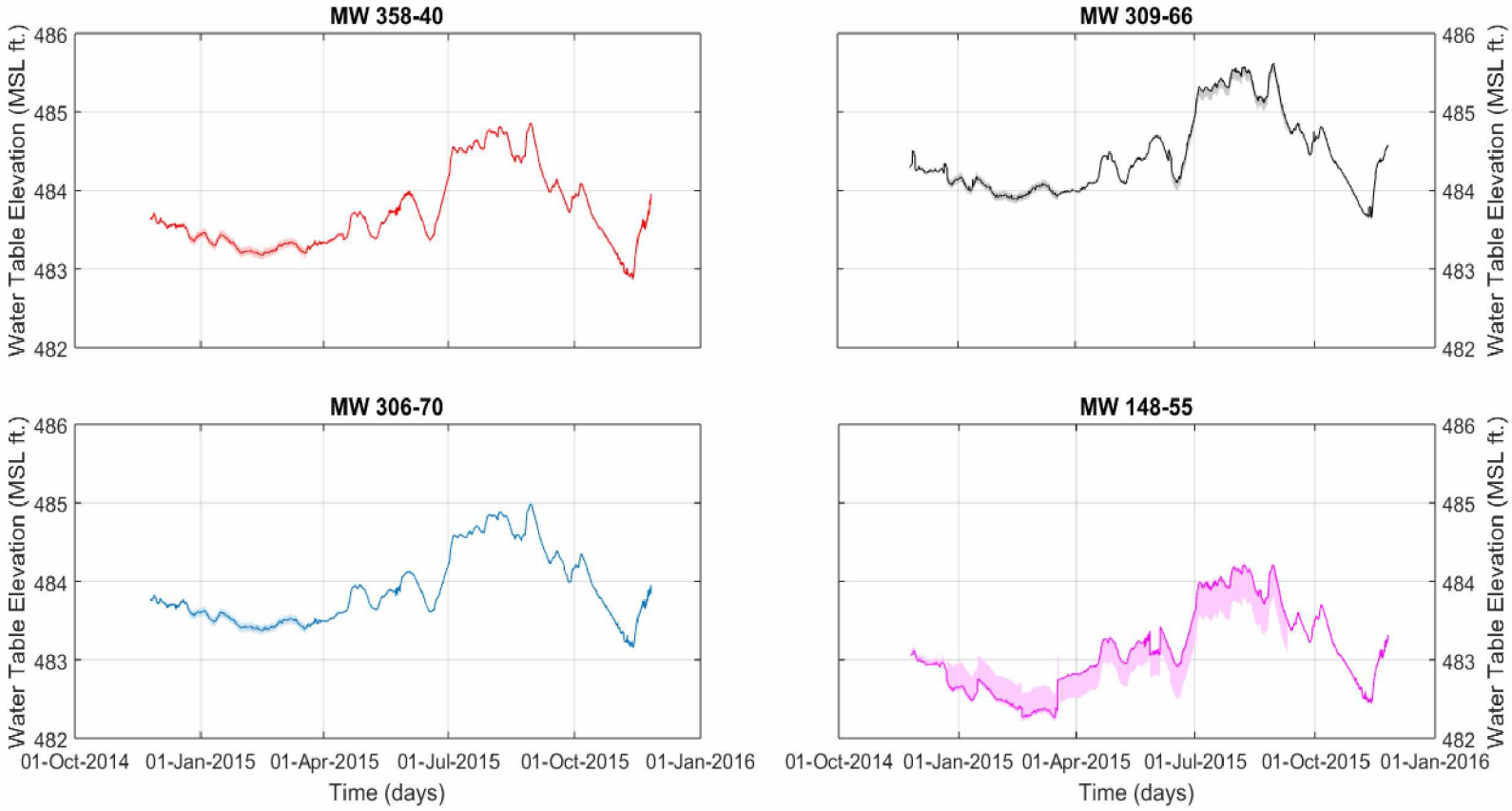

Figure 4.12 Water level Elevations with errors for mid-shallow (40 to 70 ft.) wells in Continuous Area

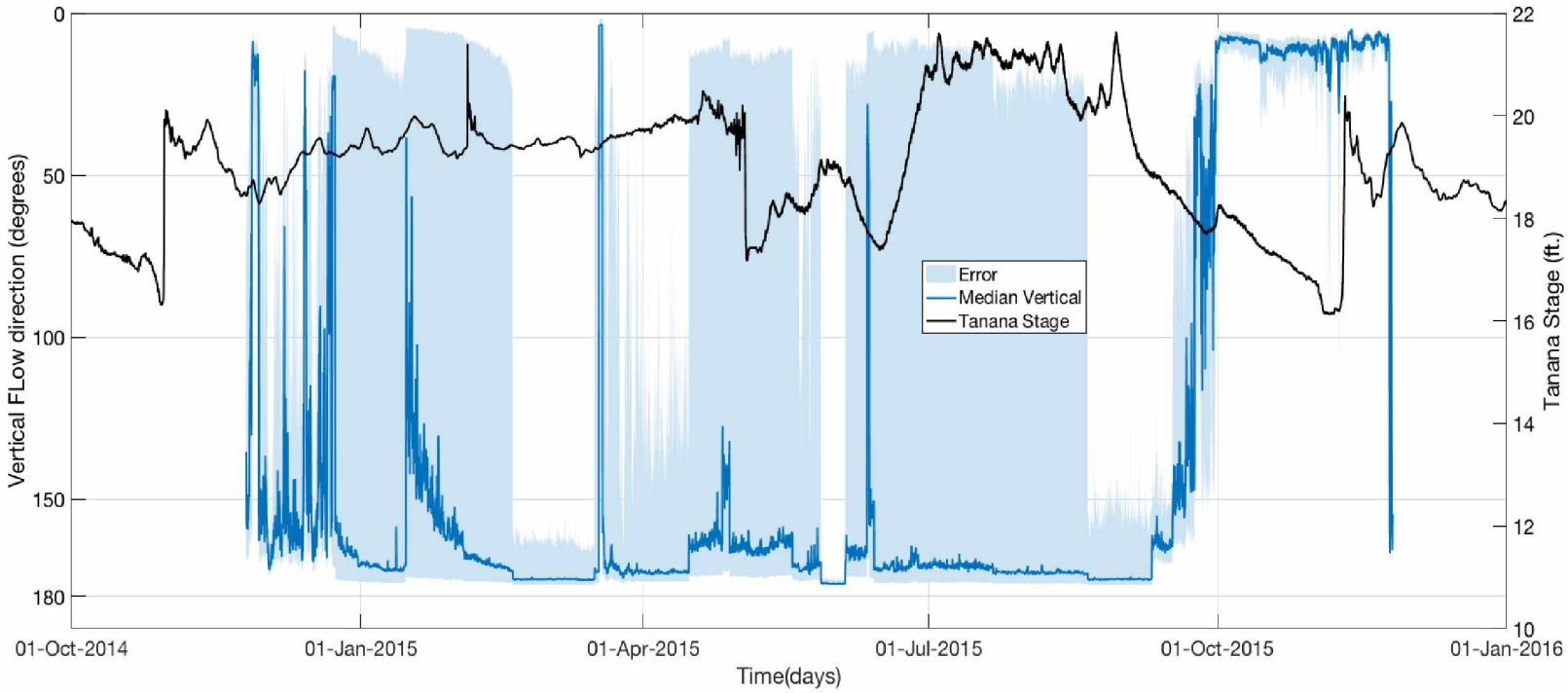

Figure 4.13 Vertical flow direction with median for mid-shallow (40 to 70 ft.) wells in Continuous Area

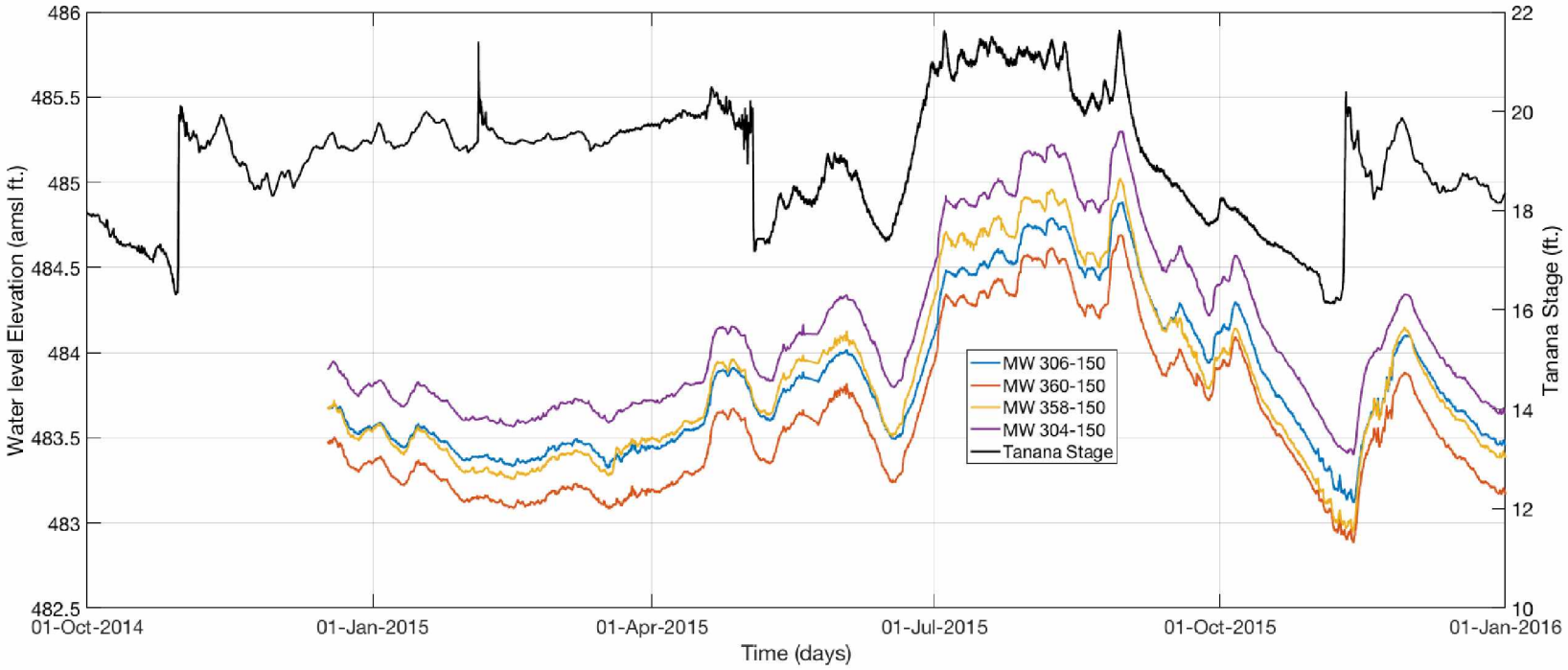

Figure 4.14 Water level Elevations for Deep (150 ft.) wells in Continuous Area

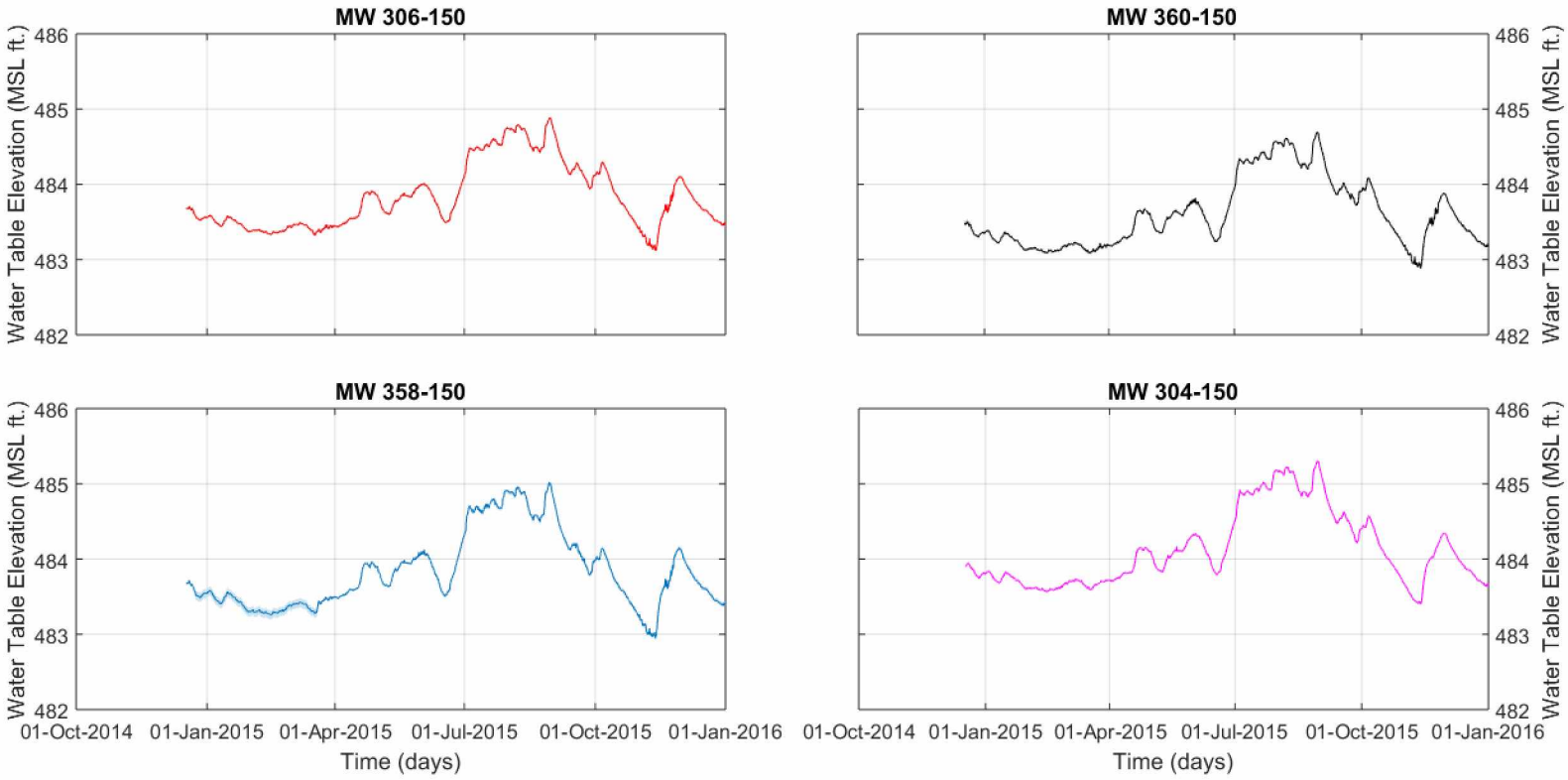

Figure 4.15 Water level Elevations with errors for deep (150 ft.) wells in Continuous Area

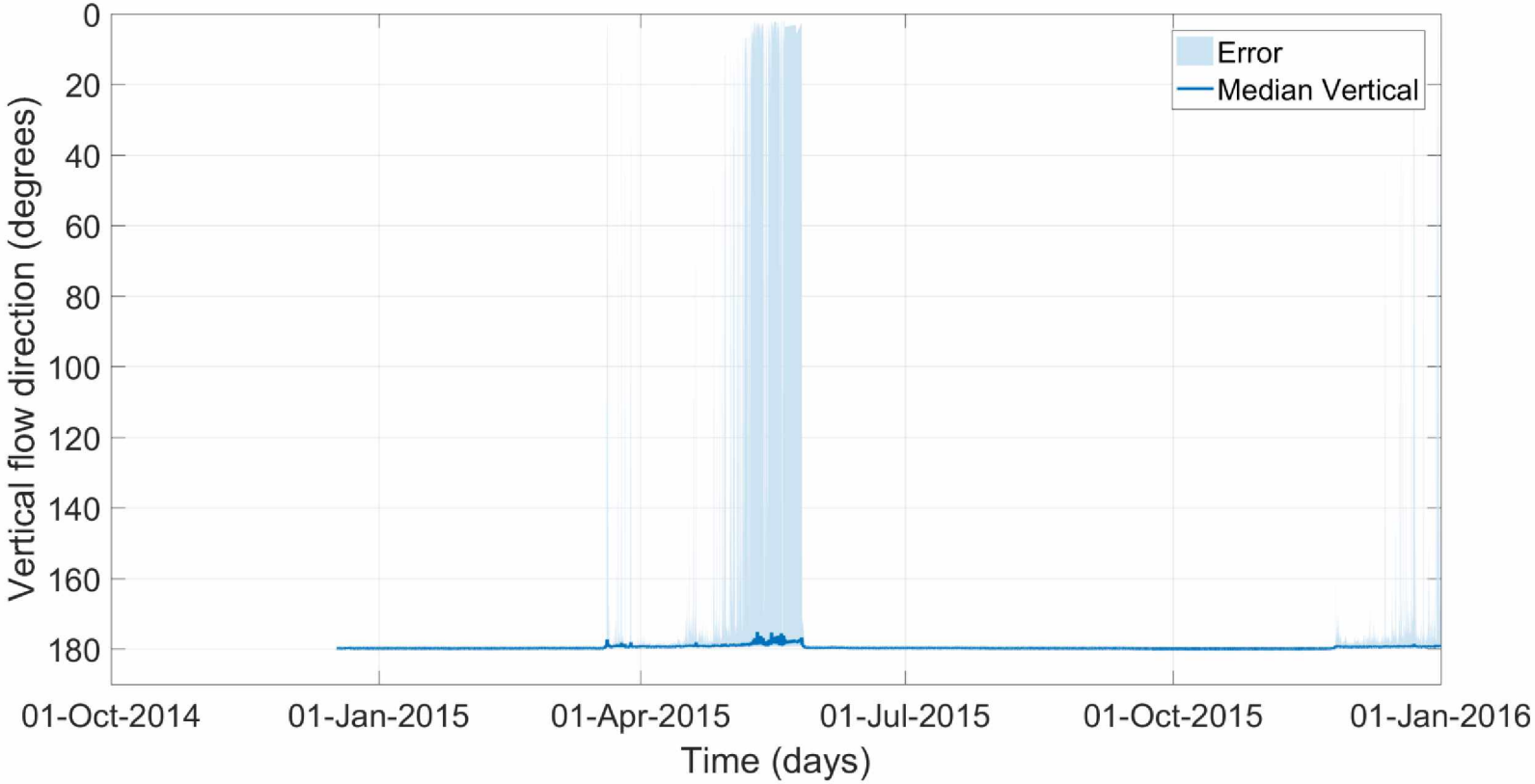

Figure 4.16 Vertical flow direction with median for deep (150 ft.) wells in Continuous Area

Chapter 5 Discussion

The objective of this study was to determine the groundwater flow directions occurring at the interface of groundwater with permafrost in a floodplain talik. An ancillary objective was to develop a method to account for water level measurement in gradient analysis. The study's hypothesis is as follows: As groundwater intersects permafrost, the flow will bifurcate where a portion of the water flows upward into the suprapermafrost portion of the aquifer and a portion is directed downward into the subpermafrost portion of the aquifer.

5.1 Vertical Component of Groundwater Flow

5.1.1 Groundwater at the interface of permafrost

Results from this research (both discrete and continuous monitored area) show that interaction of groundwater flow in a talik (floodplain talik in this study) with large permafrost zones cause the water to split into the two main portions of a discontinuous permafrost aquifer—the suprapermafrost and subpermafrost portions. The horizontal plane that separates the flow of groundwater into the suprapermafrost portion of the aquifer from the subpermafrost portion is known as the vertical groundwater divide. Results from the determination of the vertical gradient in different areas of the floodplain talik in this study indicate that the vertical groundwater divide exists between 65 and 90 ft bgs. The depth of the vertical groundwater divide varies with groundwater depth, becoming shallower to the ground surface as the water table rises and becoming deeper as the water table falls. Groundwater above the vertical groundwater divide will recharge the suprapermafrost portion of the aquifer. The subpermafrost groundwater is recharged by water flowing below the divide. The position of this divide is most likely dictated by the configuration of permafrost, specifically the somewhat vertical face of the permafrost. The

position of the divide may also change with the season. Low water levels in the aquifer, characteristic of late winter, results in a deeper (from the ground surface) position of the vertical groundwater divide. During periods of low water levels, a smaller overall percentage of the recharging water flows into the suprapermafrost portion of the aquifer. Seasonal high water levels during periods of high river stages (spring breakup and periods of high glacial melt) result in a shallower position of the divide; hence a greater percentage of the overall recharge flows into the suprapermafrost aquifer.

5.1.2 Groundwater at water table and deep wells

In the discrete monitored area, deviation from this flow pattern at the water table (downward flow instead of upward flow) is due to a falling water table. Causes for deviations in the flow pattern in the deeper portion of the aquifer (150 ft. bgs) are currently unknown.

In the continuously monitored area, the shallow and deep wells show constant upward and downward patterns, unlike the discrete area. The reason for the observed pattern might be due to the large spatial distribution of the monitoring wells which could include additional contact with permafrost topography than the discrete.

Another noticeable observation is between shallow water level depth results to the Tanana river stage. The vertical component results of shallow (15ft.) depth wells show a slight increase in trend as the Tanana River resides during the winter months (shown in Figure 4.10). A possible explanation for this might be that the Tanana is gaining groundwater during these freeze up periods. The limitation to this observation are Monte Carlo results for shallow wells of Area A. Discrete analysis shows slightly opposite by following Tanana river trend. Three possible reasons for that limitation to happen are the topography of the top permafrost, the orientation of the well clusters

as continuous area wells have closer proximity to permafrost, and finally marginal error, which in the case of Area A did show a wide range.

A crucial part of this research is to check the validity of the hypothesis and goals of the objective. With enough confidence in the results both discrete and continuous, bifurcation or groundwater divide at the interface of permafrost is analytically justified As a side note to that statement, depth of interface varies with respect to the seasonal change of groundwater levels. The combined vertical component plot of the continuous area is shown in Figure 5.1. Upward flow in water table depths, flow fluctuation at the permafrost divide, and downward direction at deep wells are examples of evidence for flow bifurcation.

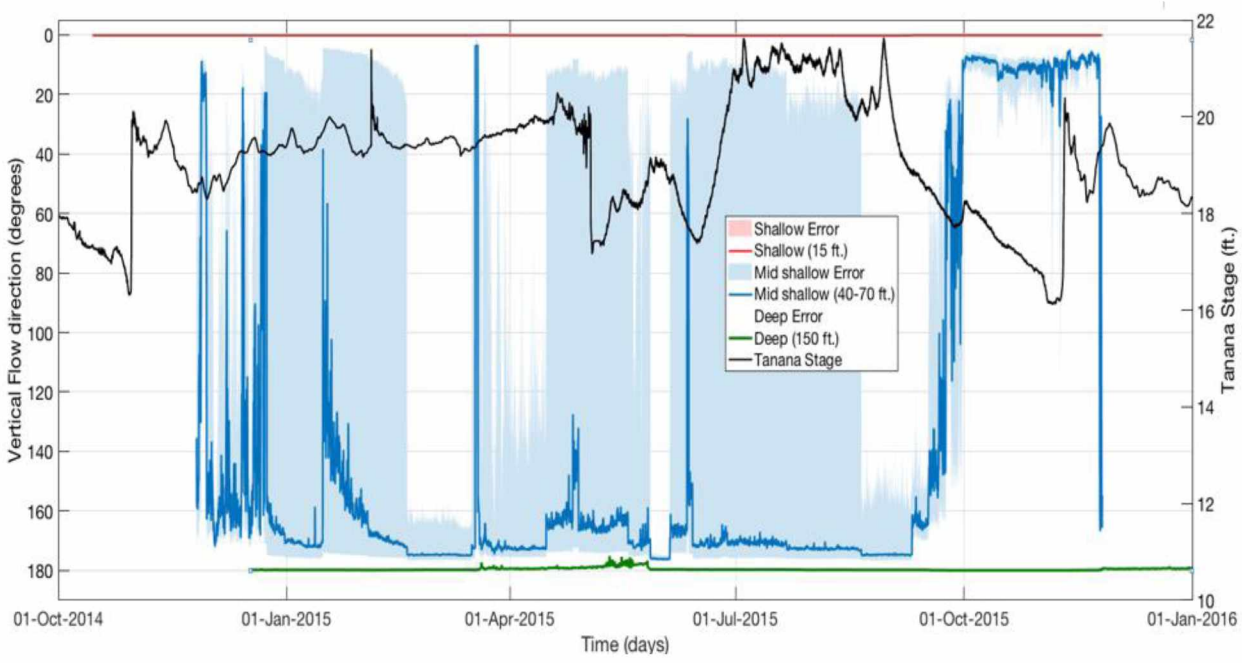

Figure 5.1 Combined plot of vertical flow direction for all the well depths in Continuous Area

5.2 Asymmetrical Error Analysis

The second major outcome of this study is the emphasis of measurement errors and the way they can alter the accuracy of the vertical flow. Previous studies by (Devlin et al., 2007; Silliman et al., 2000) showed a similar result to this study supporting the evidence that even small measurement error 0.001 ft. (0.0003m) adds a significant noise to a vertical component in three dimensions. They have used standard deviation to calculate the marginal error which is not suitable for determining the uncertainty in the flow direction and gradient magnitude. When the errors result in different positive and negative values, such as is the case when water level measurements are obtained from frost heaving and thaw subsiding monitoring wells, it would lead to an asymmetrical error problem.

A common stochastic analysis method is Monte Carlo, which is the repetitive calculation of an analytical or numerical model with different input values derived from probability distributions. Unlike the previous studies that have used Monte Carlo by standard deviation, this study determined its uncertainties by calculating the gradient magnitude and direction repetitively with Abriola et al., (1982) method using different values of total head. A simple model is created to compare the deterministic and stochastic results for symmetrical marginal errors. Table 3.12 and Figure 3.3 show the result that gives the confidence for symmetrical errors. With normally distributed results, the Monte Carlo solution provides realistic values of the marginal error in gradient and reasonable percentiles (5th and 95th) for representing the marginal error resulting from asymmetrical errors in water levels.

Study results from the Monte Carlo analyses to determine vertical flow direction often resulted in wide marginal error ranges with bimodal histograms. For different analyses, the resulting bimodal histograms show that there is a relatively high probability of upward flow (0°)

or downward flow (180°) with a low probability of a flow direction between the two extremes. Silliman et al., (2000) showed a similar result in a study on the effect of the error on the hydraulic gradient in three dimensions. These authors attribute the bimodal error extremity to the small differences between well screen elevations in the four-well pattern and the spacing between the well locations in the horizontal plane. In this study, flow at different depths from the ground surface required the selection of wells with well screen elevations that were closely spaced. Even with the resulting errors in the vertical flow direction, a majority of the bimodal histograms show a much greater probability of flow in one direction as opposed to the other, which has given confidence in conclusions on groundwater flow pattern at the interface with permafrost.

In Continuous area monitoring wells, this research took the median value as its best estimate for representing the vertical component of groundwater flow. The reason for choosing median is illustrated with a series of observations. Figure 4.12 shows the errors in water level measurements used for mid-shallow (40 to 70 ft.) depth. The vertical component of groundwater flow without considering any marginal error plotted with respect to time is shown in Figure 5.2. Even though the vertical component is in-between the 5th and 95th percentile for the period of late March 2015 through September 2015, the flow is different compared to Figure 4.13. The marginal error is evident and asymmetrical, so from the median (50th) percentile confidence interval from statistical distribution plots, the best possible estimate for the vertical component of groundwater flow direction is the median of Monte Carlo analysis.

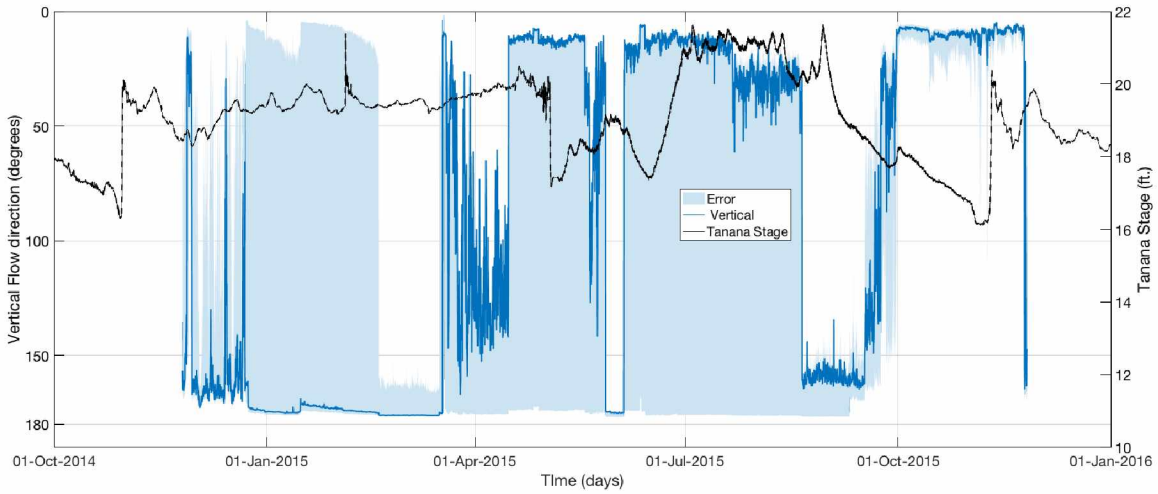

Figure 5.2 Vertical component without errors for mid-shallow wells (40 to 70 ft.)

5.3 Case Study on Research Implications

The research findings have important implications for contaminant transport in the study area. A brief description of this case study is given below.

5.3.1 Sulfolane contamination

Sulfolane is the chemical component used by the crude oil refinery to remove aromatics from the gasoline. There is a leak of the chemical in the storage unit located on the refinery site during 1980's and traces of the chemical are found beyond the refinery area including several private wells in 2009. This resulted in an extensive groundwater plume, which is approximately two miles wide, three and a half miles long, and over 300 feet deep. The chemical is highly water soluble, resistant to degradation and is well-mixed in the groundwater of the region. Sulfolane contaminated groundwater has been detected below the depth of the vertical groundwater divide, as deep as 95 ft. bgs and below since 2006; it is not known if sulfolane existed at greater depths prior to this date. To achieve the remediation, the first step is to understand how the traces of

sulfolane has reached the sub permafrost region which brings us to the study of groundwater flow of the aquifer.

5.3.2 Contaminant transport

The result from the case study shows that sulfolane had to be transported by advection below the vertical groundwater divide in order for the contaminant to reach the subpermafrost portion of the aquifer. The mechanism that caused sulfolane to move below the vertical groundwater divide was flow interaction with a small disconnected zone of permafrost. The flow pattern that is established when groundwater interacts with these small zones of permafrost is similar to the large-scale effect found in this research.

The position of the vertical groundwater divide is also important to the characterization of the contaminated aquifer. Since the vertical groundwater divide is the split between the fractions of water that flow into the two portions of the aquifer (supra and subpermafrost), it is also the divide between contaminants that migrate into the suprapermafrost groundwater and contaminants that migrate into the subpermafrost groundwater. Conceptually, if contamination exists below the groundwater divide, this contaminated groundwater will flow into the subpermafrost portion of the aquifer. If no contaminant exists below the divide, then the subpermafrost groundwater remains uncontaminated. Results show that the vertical groundwater divide exists at a depth between 65 and 90 ft. bgs. The vertical dispersion brings sulfolane contaminated groundwater below the vertical groundwater divide.

Chapter 6 Conclusion

The goal of this research was to understand that complexity of groundwater flow in discontinuous permafrost, primarily in the vertical direction, as groundwater flowing in large open taliks, such as floodplain taliks, interacts with permafrost. The study has shown that at the interaction of groundwater with the permafrost in a flood plain talik, vertical groundwater divide somewhere around 10 to 20 feet below permafrost. The depth of the vertical groundwater divide varies with groundwater depth, becoming shallower to the ground surface as the water table rises and becoming deeper as the water table falls. This gives a better understanding of fraction of water going to supra and subpermafrost groundwater. A few studies have examined the complexity of the flow pattern in 2D (horizontal). This work added the 3rd dimension, which increased the understanding of flow complexity.

The vertical direction of groundwater is sensitive to the measurement errors, which are asymmetrical. Using stochastic analysis known as Monte Carlo, the probability of the best estimate in the vertical direction is calculated. Based on the statistics, the median of the probability is determined as the reliable outcome. The hypothesis of this thesis is satisfied by the results and the implications analyzed by the case study. The contaminant transport case study provides the confidence of the finding by explaining the vertical dispersion mechanism.

Chapter 7 Future Work

The study area is limited to the number of wells and its location. Increasing the area by additional spatially distributed wells, the analysis can continue with looking at regional flow characteristics. The horizontal component of the groundwater flow is limited due to the insufficient details on permafrost topography. Further details on permafrost can help in understanding the horizontal component of the flow. The timeframe of the study is a limiting factor as well and a continued plot on the vertical component can open some new findings with changing arctic conditions.

Chapter 8 References

Abriola, L. M., & Pinder, G. F. (1982). Calculation of Velocity in 3 Space Dimensions from Hydraulic-Head Measurements. *Ground Water*, *20*(2), 205–213. http://doi.org/10.1111/j.1745-6584.1982.tb02752.x

Arcadis. (2013) Site Characterization Report December 2013, APPENDIX 5-E, Report prepared for Flint Hills Resources Alaska, LLC and North Pole Terminal, North Pole, Alaska.

Arcadis. (2014a). First Quarter 2014 Groundwater Monitoring Report prepared for Flint Hills Resources Alaska, LLC and North Pole Refinery, North Pole, Alaska.

Arcadis. (2014b). Second Quarter 2014 Groundwater Monitoring Report prepared for Flint Hills Resources Alaska, LLC and North Pole Refinery, North Pole, Alaska.

Arcadis. (2014c). Third Quarter 2014 Onsite Groundwater Monitoring Report prepared for Flint Hills Resources Alaska, LLC and North Pole Refinery, North Pole, Alaska.

Arcadis. (2014d). Fourth Quarter 2014 Onsite Groundwater Monitoring Report prepared for Flint Hills Resources Alaska, LLC and North Pole Refinery, North Pole, Alaska.

Arcadis. (2015a). First Semiannual 2015 Onsite Groundwater Monitoring Report prepared for Flint Hills Resources Alaska, LLC and North Pole Terminal, North Pole, Alaska.

Arcadis. (2015b). Second Semiannual 2015 Onsite Groundwater Monitoring Report prepared for Flint Hills Resources Alaska, LLC and North Pole Terminal, North Pole, Alaska.

Anderson, G. (1970). Hydrologic reconnaissance of the Tanana Basin, central Alaska. Retrieved from https://pubs.er.usgs.gov/publication/ha319.

Barnes, D. (2014). Detection of Discontinuities in a Discontinuous Permafrost Aquifer Using Stable Isotopes and Groundwater Temperature. *2014 NGWA Groundwater Summit*. Retrieved from https://ngwa.confex.com/ngwa/2014gws/webprogramarchives/Paper9671.html.

Bolton, W., Hinzman, L., & Yoshikawa, K. (2000). Stream flow studies in a watershed underlain by discontinuous permafrost. *Proceedings on Water Resources in Extreme ...*. Retrieved from https://scholar.google.com/scholar?q=permafrost+Hinzman+et+al.%2C+2000&btnG=&hl=en&as_sdt=0%2C2.

Brown, R. J. E. (1967). Comparison of permafrost conditions in Canada and the USSR. *Polar Record*, *13*(87), 741. http://doi.org/10.1017/S0032247400058411.

Carlson, A. E., & Barnes, D. L. (2011). Movement of trichloroethene in a discontinuous permafrost zone. *Journal of Contaminant Hydrology*, *124*(1–4), 1–13. http://doi.org/10.1016/j.jconhyd.2010.11.002.

Cederstrom, D.J., 1963. Ground-water resources of the Fairbanks area Alaska: U.S. govt. print. off. U.S. Geological SurveyWater-Supply Paper 1590. 84 p.

Circular, G. S. (n.d.). Occurrence and development of ground water in permafrost regions.

CGG. 2013. Geophysical Survey Report Airborne Magnetic and Resolve Survey, North Pole, Alaska. Prepared for Flint Hills Resource Alaska, Inc. Project 13027: 92p.

Devlin, J., & McElwee, C. (2007). Effects of measurement error on horizontal hydraulic gradient estimates. *Groundwater*. Retrieved from http://onlinelibrary.wiley.com/doi/10.1111/j.1745-6584.2006.00249.x/full.

Fienen, M. (2005). The three-point problem, vector analysis and extension to the n-point problem. *Journal of Geoscience Education*. Retrieved from http://www.nagt-jge.org/doi/abs/10.5408/1089-9995-53.3.257.

Freeze, R., & Witherspoon, P. (1967). Theoretical analysis of regional groundwater flows: 2. Effect of water-table configuration and subsurface permeability variation. *Water Resources Research*. http://onlinelibrary.wiley.com/doi/10.1029/WR003i002p00623/full.

Heginbottom, J. A., Brown, J., Humlum, O., & Svensson, H. (2012). Permafrost and periglacial environments. *State of the Earth's Cryosphere at the Beginning of the 21st Century: Glaciers, Global Snow Cover, Floating Ice, and Permafrost and Periglacial Environments*, (December), 425–496.

Hehlen, B., Courtens, E., Vacher, R., & Yamanaka, A. (2000). Hyper-Raman scattering observation of the boson peak in vitreous silica. *Physical Review*. Retrieved from https://journals.aps.org/prl/abstract/10.1103/PhysRevLett.84.5355.

Hinzman, L. D., Kane, D. L., & Woo, M. (2006). Chapter 172: Permafrost Hydrology. *Encyclopedia of Hydrological Sciences*, *2*, 1–15. http://doi.org/10.1002/0470848944.

Jorgenson, M. T., & Osterkamp, T. E. (2005). The response of boreal ecosystems to varying modes of permafrost degradation. *Canadian Journal of Forest Resources*, *35*, 2100–2111. http://doi.org/10.1139/X05-153.

Jorgenson, T., Yoshikawa, K., Kanevskiy, M., Shur, Y., Romanovsky, V., Marchenko, S., & Grosse, G. (2008). Permafrost Characteristics of Alaska. *Holocene*, 500–500.

Kraemer, T. F., & Brabets, T. P. (2012). Uranium isotopes (234 U / 238 U) in rivers of the Yukon Basin (Alaska and Canada) as an aid in identifying water sources, with implications for monitoring hydrologic change in arctic regions, 469–481. http://doi.org/10.1007/s10040-012-0829-3.

Lawson, D., Strasser, J., Strasser, J., & Arcone, S. (1996). Geological and geophysical investigations of the hydrogeology of Fort Wainwright, Alaska.

Mandel, J.1964. The Statistical Analysis of Experimental Data. Dover Publications: 410p.

Mckenzie, J. M., & Voss, C. I. (2013). Permafrost thaw in a nested groundwater- fl ow system. *Springer*, *21*, 299–316. http://doi.org/10.1007/s10040-012-0942-3.

Mikhailov, V. (2008). Convective heat exchange between rivers and floodplain taliks. *Proceedings of the 9th International Conference on*. Retrieved from https://scholar.google.com/scholar?hl=en&q=Convective+Heat+Exchange+Between+Rivers+and+Floodplain+Taliks&btnG=&as_sdt=1%2C2&as_sdtp.

Pinder, G., Celia, M., & Gray, W. (1981). Velocity calculation from randomly located hydraulic heads. *Groundwater*. Retrieved from http://onlinelibrary.wiley.com/doi/10.1111/j.1745-6584.1981.tb03468.x/full.

Reger, R., & Péwé, T. (1976). Cryoplanation terraces: indicators of a permafrost environment. *QuaternaryResearch*. http://www.sciencedirect.com/science/article/pii/0033589476900429.

Shannon and Wilson. 2013. Standard Operating Procedures (SOP) for Groundwater-Elevation Monitoring. Prepared by Shannon and Wilson, Inc., Fairbanks, Alaska, July 25: 7p.

Silliman, S., & Frost, C. (1998). Monitoring hydraulic gradient using three-point estimator. *Journal of Environmental Engineering*. Retrieved from http://ascelibrary.org/doi/abs/10.1061/(ASCE)0733-9372(1998)124:6(517).

Silliman, S., & Mantz, G. (2000). The effect of measurement error on estimating the hydraulic gradient in three dimensions. *Groundwater*. Retrieved from http://onlinelibrary.wiley.com/doi/10.1111/j.1745-6584.2000.tb00208.x/full.

Sloan, C., & Everdingen, R. van. (1988). Region 28, permafrost region. *The Geology of North America*. Retrieved from http://www.clemson.edu/ces/hydro/murdoch/Courses/Aquifer Systems/documents/Heath and Back books/Chapter 31.pdf.

Taylor, J.R. 1997. An Introduction to Error Analysis: The Study of Uncertainties in Physical Measurements. University Science Books: 327p

Vacher, H. (1989). The three-point problem in the context of elementary vector analysis. *Journal of Geological Education*. Retrieved from http://www.nagt-jge.org/doi/abs/10.5408/0022-1368-37.4.280.

Walvoord, M. A., Voss, C. I., & Wellman, T. P. (2012). Influence of permafrost distribution on groundwater flow in the context of climate-driven permafrost thaw: Example from Yukon Flats Basin, Alaska, United States. *Water Resources Research*, *48*(7), 1–17. http://doi.org/10.1029/2011WR011595.

Williams, R. (1970). Groundwater flow systems and accumulation of evaporite minerals. *AAPG Bulletin*.http://archives.datapages.com/data/bulletns/196870/data/pg/0054/0007/1250/1290.